PHYSICAL REVIEW D **91,** 035026 (2015)

Confronting the moduli-induced lightest-superpartner problem

Nikita Blinov,[1,2,*] Jonathan Kozaczuk,[1,†] Arjun Menon,[3,‡] and David E. Morrissey[1,§]

[1]*Theory Department, TRIUMF, 4004 Wesbrook Mall, Vancouver, British Columbia V6T 2A3, Canada*

[2]*Department of Physics and Astronomy, University of British Columbia, Vancouver, British Columbia V6T 1Z1, Canada*

[3]*Department of Physics, University of Oregon, Eugene, Oregon 97403, USA*

(Received 24 September 2014; published 25 February 2015)

Moduli fields with Planck-suppressed couplings to light species are common in string compactifications. Decays of these moduli can reheat the Universe at a late time and produce dark matter nonthermally. For generic moduli fields motivated by string theory with masses similar to that of the gravitino and TeV-scale superpartners in the minimal supersymmetric Standard Model (MSSM), the nonthermal production of the lightest superpartner (LSP) tends to create an unacceptably large relic density or too strong of an indirect detection signal. We call this the moduli-induced LSP problem of the MSSM. In this paper we investigate extensions of the MSSM containing new LSP candidates that can alleviate this tension. We examine the viability of this scenario in models with light Abelian and non-Abelian hidden sectors and symmetric or asymmetric dark matter. In these extensions it is possible, though somewhat challenging, to avoid a moduli-induced LSP problem. In all but the asymmetric scenario, the LSP can account for only a small fraction of the observed dark matter density.

DOI: 10.1103/PhysRevD.91.035026 PACS numbers: 12.60.Jv, 12.60.-i, 95.35.+d, 98.80.Cq

I. INTRODUCTION

Moduli are light scalar fields with only higher-dimensional couplings to other light species. They arise frequently in theories with supersymmetry [1–3], and they appear to be a generic feature of string compactifications [4–6]. Moduli fields can also have significant implications for the cosmological history of the Universe, the mass spectrum of the supersymmetric partners of the Standard Model (SM), and the density of dark matter (DM) today [7–9].

A modulus field can alter the standard cosmology if it is significantly displaced from the minimum of its potential in the early Universe, as can occur following primordial inflation [10]. The modulus will be trapped by Hubble damping until $H \sim m_\varphi$, at which point it will begin to oscillate. The energy density of these oscillations dilutes in the same way as nonrelativistic matter and can easily come to dominate the expansion of the Universe.[1] This will continue until the modulus decays at time $t \sim \Gamma_\varphi^{-1}$, transferring the remaining oscillation energy into radiation. At this point, called *reheating*, the radiation temperature is approximately [16]

$$T_{\rm RH} \sim (5\ {\rm MeV}) \left(\frac{M_{\rm Pl}}{\Lambda}\right) \left(\frac{m_\varphi}{100\ {\rm TeV}}\right)^{3/2}, \qquad (1)$$

where Λ is the heavy mass scale characterizing the coupling of the modulus to light matter. To avoid disrupting primordial nucleosynthesis, the reheating temperature should be greater than about $T_{\rm RH} \gtrsim 5$ MeV [17], and this places a lower bound on the modulus mass.

The mass of a modulus field is determined by its potential. In string compactifications, multiple moduli typically appear in the low-energy supergravity theory as components of chiral multiplets with couplings to other fields suppressed by powers of $\Lambda \sim M_{\rm Pl}$ [6]. While the potentials of many of these moduli are not completely understood, certain features do seem to be fairly universal. For example, moduli masses of $m_\varphi \sim m_{3/2}$ are expected when the potential arises mainly from supersymmetry breaking [18]. Moduli may also have supersymmetric potentials [19], and $m_\varphi \gg m_{3/2}$ is found in some cases [20,21]. However, $m_\varphi \sim m_{3/2}$ is still frequently obtained from supersymmetric potentials once the constraint of a very small vacuum energy is imposed [21]. Thus, a plausible generic expectation from string theory is that there exists at least one modulus field with $m_\varphi \sim m_{3/2}$ and $\Lambda \sim M_{\rm Pl}$ [6].[2] Other heavier moduli may be present, but since the lightest and most weakly coupled modulus will decay the latest, it is expected to have the greatest impact on the present-day cosmology.

Putting these two pieces together, acceptable reheating from string moduli suggests $m_\varphi \sim m_{3/2} \gtrsim 100$ TeV. This has important implications for the masses of the SM superpartner fields. Surveying the most popular mechanisms

*nblinov@triumf.ca
†jkozaczuk@triumf.ca
‡aamenon@uoregon.edu
§dmorri@triumf.ca

[1]Such an early matter-dominated phase might also leave an observable signal in gravitational waves at multiple frequencies [11] or modify cosmological observables [12–15].

[2]The LARGE Volume Scenario of Refs. [22,23] is a notable exception to this.

of supersymmetry-breaking mediation [24], the typical size of the superpartner masses is

$$m_{\rm soft} \sim \begin{cases} m_{3/2} & \text{gravity mediation} \\ (\frac{LM_{\rm Pl}}{M_*})m_{3/2} & \text{gauge mediation} \\ Lm_{3/2} & \text{anomaly mediation} \end{cases}, \quad (2)$$

where $L \sim g^2/(4\,\pi)^2$ is a typical loop factor and $M_* \ll M_{\rm Pl}/L$ is the mass of the gauge messengers. Of these mechanisms, only anomaly mediation (AMSB) allows for superpartners that are light enough to be directly observable at the Large Hadron Collider (LHC) [25,26]. Contributions to the soft terms of similar size can also be generated by the moduli themselves [27,28] or other sources [29–32]. However, for these AMSB and AMSB-like contributions to be dominant, the gravity-mediated contributions must be suppressed [25], which is nontrivial for the scalar soft masses [33–37]. An interesting intermediate scenario is minisplit supersymmetry where the dominant scalar soft masses come from direct gravity mediation with $m_{\rm soft} \sim m_{3/2}$, while the gaugino soft masses are AMSB-like [38–43].

Moduli reheating can also modify dark matter production [16,44–47]. A standard weakly interacting massive particle (WIMP) χ will undergo thermal freeze-out at temperatures near $T_{\rm fo} \sim m_\chi/20$. If this is larger than the reheating temperature, the WIMP density will be strongly diluted by the entropy generated from moduli decays. On the other hand, DM can be created *nonthermally* as moduli decay products. A compelling picture of nonthermal dark matter arises very naturally for stringlike moduli and an AMSB-like superpartner mass spectrum [16]. The lightest (viable) superpartner (LSP) in this case tends to be a winolike neutralino. These annihilate too efficiently to give the observed relic density through thermal freeze-out [48–50]. However, with moduli domination and reheating, the wino LSP can be created nonthermally in moduli decays, and the correct DM density is obtained for $M_2 \sim 200$ GeV and $m_\varphi \sim 3000$ TeV.

This scenario works precisely because the wino annihilation cross section is larger than what is needed for thermal freeze-out. Unfortunately, such enhanced annihilation rates are strongly constrained by gamma ray observations of the Galactic center by Fermi and HESS, and the nonthermal wino is ruled out even for very conservative assumptions about the DM profile in the inner galaxy (e.g. cored isothermal) [49,50]. A winolike LSP can be consistent with these bounds if it is only a subleading component of the total DM density. Using the AMSB relation for M_2 in terms of $m_{3/2}$, this forces $m_\varphi/m_{3/2} \gtrsim 100$, significantly greater than the generic expectation [50]. The problem is even worse for other neutralino LSP species, since these annihilate less efficiently and an even larger value of $m_\varphi \gg m_{3/2}$ is needed to obtain an acceptable relic density. Furthermore, $m_\varphi > 2m_{3/2}$ also allows the modulus field to decay to pairs of gravitinos. The width for this decay is typically similar to the total width to SM superpartners [51–54]. For $m_\varphi \gg m_{3/2} > 30$ TeV, the gravitinos produced this way will decay to particle-superpartner pairs before nucleosynthesis but after the modulus decays, and recreate the same LSP density problem that forced $m_\varphi \gg m_{3/2}$ in the first place.

These results suggest a degree of tension between reheating by string-motivated moduli (with $m_\varphi \sim m_{3/2}$ and $\Lambda \sim M_{\rm Pl}$) and the existence of a stable TeV-scale LSP in the minimal supersymmetric standard model (MSSM). This tension can be resolved if all relevant moduli have properties that are slightly different from the naïve expectation; for example $m_\varphi \gg m_{3/2}$ and $\mathrm{BR}(\varphi \to \psi_{3/2}\psi_{3/2}) \ll 1$ [54,55], an enhanced modulus decay rate with $m_\varphi \sim m_{3/2}$ and $\Lambda < M_{\rm Pl}$ [56], or a suppressed modulus branching fraction into superpartners [57]. Given the challenges and uncertainties associated with moduli stabilization in string theory, we focus on what seem to be more generic moduli and we investigate a second approach: extensions of the MSSM that contain new LSP candidates with smaller relic densities or that are more difficult to detect than their MSSM counterparts.

In this paper we investigate extensions of the MSSM containing additional hidden gauge sectors as a way to avoid the moduli-induced LSP problem of the MSSM. Such gauge extensions arise frequently in grand-unified theories [58] and string compactifications [59,60]. We assume that the dominant mediation of supersymmetry breaking to gauginos is proportional to the corresponding gauge coupling, as in anomaly or gauge mediation, allowing the hidden sector gauginos to be lighter than those of the MSSM if the former have a smaller coupling constant [61–63]. We also focus on the case of a single light modulus field with $m_\varphi \sim m_{3/2}$ and $\Lambda \sim M_{\rm Pl}$, although similar results are expected to hold for multiple moduli or for reheating by gravitino decays.

This paper is organized as follows. In Sec. II we review moduli cosmology and the resulting nonthermal production of LSPs. Next, in Sec. III we examine in more detail the tension between moduli reheating and a stable MSSM LSP. In the subsequent three sections we present three extensions of the MSSM containing new LSP candidates and examine their abundances and signals following moduli reheating. The first extension, discussed in Sec. IV, comprises a minimal supersymmetric $U(1)_x$ hidden sector. We find that this setup allows for a hidden sector LSP with a relic density lower than that of the wino and which is small enough to evade the current bounds from indirect detection. In Sec. V we extend the $U(1)_x$ hidden sector to include an asymmetric dark matter candidate and find that it is able to saturate the entire observed DM relic density while avoiding constraints from indirect detection. In Sec. VI we investigate a pure non-Abelian hidden sector, and show that

the corresponding gaugino LSP can provide an acceptable relic density and avoid constraints from indirect detection, although it is also very strongly constrained by its effect on structure formation and the cosmic microwave background. Finally, Sec. VII is reserved for our conclusions.

II. MODULI REHEATING AND DARK MATTER

In this section we review briefly the cosmology of moduli oscillation and decay, as well as the associated nonthermal production of dark matter.

A. Moduli reheating

A modulus field φ is very likely to develop a large initial displacement from the minimum of its potential before or during the course of primordial inflation [1,10]. Hubble damping will trap the modulus until $H \sim m_\varphi$, at which point it will start to oscillate coherently. For even moderate initial displacements, these oscillations will eventually dominate over radiation. The time evolution of the modulus oscillation energy density for $H < m_\varphi$ is given by

$$\dot{\rho}_\varphi + 3\,H\rho_\varphi + \Gamma_\varphi \rho_\varphi = 0, \tag{3}$$

where Γ_φ is the modulus decay rate. For a modulus field with $M_{\rm Pl}$-suppressed couplings,

$$\Gamma_\varphi = \frac{c}{4\,\pi}\frac{m_\varphi^3}{M_{\rm Pl}^2}, \tag{4}$$

where c is a model-dependent number with a typical range of $10^{-3} < c < 100$ [50].[3] As the modulus oscillates, it decays to radiation with the radiation density becoming dominant once more when $H \sim \Gamma_\varphi$.

The evolution of the radiation density ρ_R follows from the first law of thermodynamics,

$$\frac{d\rho_R}{dt} + 3\,H(\rho_R + p_R) = \Gamma_\varphi \rho_\varphi, \tag{5}$$

where p_R is the radiation pressure. The right-hand side is the rate of energy injection into the bath, of which moduli decays are assumed to be the dominant source. Contributions from DM annihilation can also be included, but these do not make much difference when the DM is lighter than the modulus field. The radiation density is used to define the temperature through

$$\rho_R = \frac{\pi^2}{30} g_*(T) T^4, \tag{6}$$

where $g_*(T)$ is the effective number of relativistic degrees of freedom [64]. Reheating is said to occur when radiation becomes the dominant energy component of the Universe, corresponding to $H(T_{\rm RH}) \simeq \Gamma_\varphi$. Following Refs. [16], we define the reheating temperature $T_{\rm RH}$ to be

$$T_{\rm RH} = \left(\frac{90}{\pi^2 g_*(T_{\rm RH})}\right)^{1/4} \sqrt{\Gamma_\varphi M_{\rm Pl}} \simeq (5.6\ {\rm MeV})\, c^{1/2} \left(\frac{10.75}{g_*}\right)^{1/4} \left(\frac{m_\varphi}{100\ {\rm TeV}}\right)^{3/2}. \tag{7}$$

Here $M_{\rm Pl} \simeq 2.4 \times 10^{18}$ GeV is the reduced Planck mass. The reheating temperature $T_{\rm RH}$ should exceed 5 MeV to preserve the predictions of primordial nucleosynthesis [17].[4] For $c = 1$ this implies that $m_\varphi \gtrsim 100$ TeV.

B. Nonthermal dark matter

Moduli decays can also produce stable massive particles, such as a self-conjugate dark matter candidate χ [16]. This is described by

$$\frac{dn_\chi}{dt} + 3Hn_\chi = \frac{\mathcal{N}_\chi \Gamma_\varphi}{m_\varphi}\rho_\varphi - \langle\sigma v\rangle (n_\chi^2 - n_{\rm eq}^2), \tag{8}$$

where $\langle\sigma v\rangle$ is the thermally averaged annihilation cross section, $n_{\rm eq} = g T m_\chi^2 K_2(m_\chi/T)/2\pi^2$ is the equilibrium number density, with g being the number of internal degrees of freedom, and $\mathcal{N}_\chi$ is the average number of χ particles produced per modulus decay.[5] Values of $\mathcal{N}_\chi \sim 1$ are usually expected when χ is the LSP [18,66]. Together, Eqs. (3), (5), and (8) and the Friedmann equation form a closed set of equations for the system.

The general solution of these equations interpolates between three distinct limits [16,44,46]. For reheating temperatures above the thermal freeze out temperature $T_{\rm fo}$ of χ, the final χ density approaches the thermal value. When $T_{\rm RH} < T_{\rm fo}$, annihilation may or may not be significant depending on $\langle\sigma v\rangle$ and $\mathcal{N}_\chi$. Smaller values imply negligible χ annihilation after reheating and a final relic density of about [46]

$$\Omega_\chi h^2 \simeq \frac{3}{4}\mathcal{N}_\chi \left(\frac{m_\chi}{m_\varphi}\right) T_{\rm RH} \left(\frac{s_0}{\rho_c/h^2}\right) \simeq (1100)\mathcal{N}_\chi \left(\frac{m_\chi}{100\ {\rm GeV}}\right)\left(\frac{T_{\rm RH}}{5\ {\rm MeV}}\right)\left(\frac{100\ {\rm TeV}}{m_\varphi}\right), \tag{9}$$

where s_0 is the entropy density today and ρ_c/h^2 is the critical density. Larger values of $\mathcal{N}_\chi$ or $\langle\sigma v\rangle$ lead to

[3] Values of c much larger than this can be interpreted as corresponding to a suppression scale $\Lambda < M_{\rm Pl}$.

[4] We have adjusted for our slightly different definition of $T_{\rm RH}$ relative to Ref. [17] in the quoted bound.

[5] This includes χ produced in direct decays, as well as rescattering [65] and decay cascades.

significant annihilation among the χ during the reheating process, giving a relic density of [45,46]

$$\begin{aligned}\Omega_\chi h^2 &\simeq \frac{m_\chi \Gamma_\varphi}{\langle\sigma v\rangle s_{\rm RH}}\left(\frac{s_0}{\rho_c/h^2}\right)\\ &\simeq (0.2)\left(\frac{m_\chi/20}{T_{\rm RH}}\right)\left(\frac{3\times10^{-26}\ {\rm cm}^3/{\rm s}}{\langle\sigma v\rangle}\right)\left(\frac{10.75}{g_*}\right)^{1/2}\\ &\simeq (200)c^{-1/2}\left(\frac{m_\chi}{100\ {\rm GeV}}\right)\left(\frac{3\times10^{-26}\ {\rm cm}^3/{\rm s}}{\langle\sigma v\rangle}\right)\\ &\quad\times\left(\frac{100\ {\rm TeV}}{m_\varphi}\right)^{3/2}\left(\frac{10.75}{g_*}\right)^{1/4}. \end{aligned} \tag{10}$$

We emphasize that the expressions of Eqs. (9) and (10) are only approximations valid to within a factor of order unity. In what follows we solve this system numerically using the methods of Refs. [67,68]. For $T_{\rm RH} < T_{\rm fo}$ and $\mathcal{N}_\chi$ not too small, the reannihilation scenario is usually the relevant one [46].

C. Scaling relations

It is instructive to look at how the relation of Eq. (10) scales with the relevant couplings and masses [61]. Motivated by the MSSM wino in anomaly mediation, we will assume that the dark matter mass scales with a coupling g_χ according to

$$m_\chi = r_\chi \frac{g_\chi^2}{(4\ \pi)^2} m_{3/2}, \tag{11}$$

for some parameter r_χ. We will assume further that the dark matter annihilation cross section scales with the coupling as well,

$$\langle\sigma v\rangle = \frac{k_\chi}{4\pi}\frac{g_\chi^4}{m_\chi^2}, \tag{12}$$

for some parameter k_χ. For an AMSB-like wino, the r and k parameters are [16]

$$r_2 \simeq 1, \tag{13}$$

$$k_2 \simeq 2\frac{[1-(m_W/M_2)^2]^{3/2}}{[2-(m_W/M_2)^2]^2} \to 1/2, \tag{14}$$

with $g_\chi = g_2 \simeq 0.65$, and the last expression neglects coannihilation with charginos, which can be suppressed at low reheating temperatures [46].

With these assumptions, the thermal χ abundance is

$$\begin{aligned}\Omega_\chi^{\rm th} h^2 &\simeq (5.5\times10^{-3})\frac{r_\chi^2}{k_\chi}\left(\frac{m_\chi/T_{\rm fo}}{20}\right)\left(\frac{m_{3/2}}{100\ {\rm TeV}}\right)^2\\ &\quad\times\left(\frac{106.75}{g_*}\right)^{1/2}, \end{aligned} \tag{15}$$

independent of the specific mass or coupling. This is no longer true of nonthermal DM produced by moduli decays, where the mass dependence is different. Rewriting Eq. (10) subject to the assumptions of Eqs. (11) and (12), we obtain

$$\begin{aligned}\Omega_\chi h^2 &\simeq 15c^{-1/2}\left(\frac{r_\chi^3/k_\chi}{r_2^3/k_2}\right)\left(\frac{g_\chi}{g_2}\right)^2\left(\frac{m_{3/2}}{m_\varphi}\right)^3\left(\frac{m_\varphi}{100\ {\rm TeV}}\right)^{3/2}\\ &\quad\times\left(\frac{10.75}{g_*}\right)^{1/4}. \end{aligned} \tag{16}$$

This result shows that reducing the coupling or the modulus mass suppresses the nonthermal relic density. It also makes clear that $m_\varphi > m_{3/2}$ is needed to obtain an acceptable wino abundance within the reannihilation regime.

D. Gravitino production and decay

Our previous discussion of moduli reheating did not take gravitinos into account. Moduli can also decay to gravitinos if $m_\varphi > 2m_{3/2}$, and the corresponding branching ratio ${\rm BR}_{3/2}$ is expected to be on the order of unity unless some additional structure is present [51–54]. For $m_\varphi \sim 2m_{3/2}$, the gravitinos will decay at about the same time as the moduli and our previous results for the moduli-only case are expected to apply here as well. On the other hand, if $m_\varphi \gg m_{3/2}$ and ${\rm BR}_{3/2}$ is not too small, the gravitinos produced by decaying moduli are likely to come to dominate the energy density of the Universe before they themselves decay. We examine this possibility here, and show that our results for moduli decay can be applied to this scenario as well after a simple reinterpretation of parameters.

If the gravitino is not the LSP, it will decay to lighter particle-superpartner pairs with

$$\Gamma_{3/2} = \frac{d}{4\pi}\frac{m_{3/2}^3}{M_{\rm Pl}^2}, \tag{17}$$

where $d = 193/96$ if all MSSM final states are open and $d = (1+3+8)/8 = 3/2$ if only gaugino modes are available [69]. These decays will not appreciably disrupt BBN for $m_{3/2} \gtrsim 30$ TeV, but they can produce a significant amount of LSP dark matter.

For $m_\varphi \gg m_{3/2}$, the modulus will decay much earlier than the gravitino (unless $c \ll d$). The gravitinos produced by moduli decays at time $t_i \simeq \Gamma_\varphi^{-1}$ will be initially relativistic with $p/m_{3/2} = m_\varphi/2m_{3/2}$. Their momentum will redshift with the expansion of the Universe, and they will become nonrelativistic at time

$$t_{\rm nr} \simeq \frac{d}{4c}\left(\frac{m_{3/2}}{m_\varphi}\right)\Gamma_{3/2}^{-1}, \tag{18}$$

where we have assumed that the Universe is radiation dominated after moduli reheating. Thus, the gravitinos produced in moduli decays become nonrelativistic long

before they decay for $m_{3/2}/m_\varphi \ll 1$ (and $c \sim d$). While $t_{\rm nr} < t < \Gamma_{3/2}^{-1}$, the gravitinos will behave like matter. The quantity $m_{3/2}n_{3/2}$ begins to exceed the (nongravitino) radiation density at time

$$t \simeq \frac{d}{c}\left(\frac{1-\mathrm{BR}_{3/2}}{\mathrm{BR}_{3/2}}\right)^2\left(\frac{m_{3/2}}{m_\varphi}\right)^3\Gamma_{3/2}^{-1}. \tag{19}$$

Again, this is much earlier than the gravitino decay time for $m_{3/2}/m_\varphi \ll 1$ unless $\mathrm{BR}_{3/2}$ or c/d is suppressed.[6]

The scenario that emerges for $m_{3/2} \ll m_\varphi$, $c \sim d$, and $\mathrm{BR}_{3/2} \sim 1$ is very similar to a second stage of moduli reheating: the gravitinos produced in moduli decays become nonrelativistic and come to dominate the energy density of the Universe until they decay at time $t \simeq \Gamma_{3/2}^{-1}$, at which point they reheat the Universe again. Dark matter will also be created by the gravitino decays, with at least one LSP produced per decay (assuming R-parity conservation). The large gravitino density from moduli decays can interfere with nucleosynthesis or produce too much dark matter, and is sometimes called the moduli-induced gravitino problem [51–54].

We will not discuss gravitinos much for the remainder of this paper. Instead, we will focus mainly on the case of $m_\varphi \sim m_{3/2}$, where the presence of gravitinos does not appreciably change our results [46]. However, our findings can also be applied to scenarios with $m_\varphi \gg m_{3/2}$, $c \sim d$, and $\mathrm{BR}_{3/2} \sim 1$ with the moduli decays reinterpreted as gravitino decays (i.e. $m_\varphi \to m_{3/2}$, $c \to d$, $\mathcal{N}_\chi \to 1$).

III. MODULI REHEATING AND THE MSSM

The discussion of Sec. II shows that the LSP relic density is enhanced in the moduli-decay scenario relative to thermal freeze out unless the fraction of decays producing LSPs $\mathcal{N}_\chi$ is very small. In Ref. [50], this observation was used to put a very strong constraint on winolike LSPs produced by moduli decays. In this section we apply these results to more general MSSM neutralino LSPs, and we argue that the MSSM has a *moduli-induced LSP problem* for $m_\varphi \sim m_{3/2}$, $c \sim 1$, and $\mathcal{N}_\chi$ not too small. See also Refs. [70,71] for related analyses.

Consider first a winolike LSP with an AMSB-like mass. Direct searches at the LHC imply that the mass must lie above $m_{\chi_1^0} \gtrsim 270$ GeV if it is nearly pure wino [72], although smaller masses down to the LEP limit $m_{\chi_1^\pm} \gtrsim 104$ GeV are possible if it has moderate mixing with a Higgsino [73]. Examining Eq. (16), the moduli-induced wino relic density (in the reannihilation regime) tends to be larger than the observed DM density, and indirect detection places an even stronger bound of $\Omega_\chi h^2 \lesssim 0.05$ [50]. Fixing $m_\chi = 270$ GeV, a relic density of this size can be obtained with the very optimistic combination of parameter values $c = 100$, $m_\varphi = 2m_{3/2}$, and $r_\chi/r_2 \lesssim 0.3$. Such a reduction in r_χ/r_2 can arise from supersymmetry-breaking threshold corrections [74,75] or moduli-induced effects [27,28], but requires a significant accidental cancellation relative to the already-small AMSB value of r_2 [50].

A small effective value of $r_\chi < r_2$ could also arise from $|\mu| \ll |M_2|$ and a corresponding Higgsino-like LSP. The reduction in the relic density in this case is countered by a smaller annihilation cross section: for $\mu \gg m_W$, heavy scalars, and neglecting coannihilation, we have $g_\chi \simeq g_2$, $r_\chi = (\mu/M_2)$, and $k_\chi \simeq (3 + 2t_W^2 + t_W^4)/128 \simeq 0.03$ [48] (where $t_W \equiv \tan\theta_W$, with θ_W the Weinberg angle). To investigate this possibility in more detail, we set $m_\varphi/m_{3/2} = 1, 10, 100$ and $c = 1$, and compute the moduli-induced LSP relic density for various values of μ/M_2 and $m_{3/2}$. In doing so, we fix M_2 to its AMSB value with $c = 1$ and $m_\varphi = m_{3/2}$, and we compute the annihilation cross section in DarkSUSY [76,77]. For the other MSSM parameters, we set $\tan\beta = 10$, $m_A = 1000$ GeV, $\tilde{m} = 2000$ GeV for all scalars, and we fix A_t such that $m_h = 126 \pm 1$ GeV.

Fixing $m_\varphi/m_{3/2} = 1, 10$ we find no Higgsino-like points with $\Omega_\chi h^2 \leq 0.12$, i.e. for values which would appear to be generically expected from string theory.[7] Smaller relic densities are found for $m_\varphi/m_{3/2} = 100$, and the results of our scan for this ratio are shown in Fig. 1. The LSP relic density is smaller than the total DM density to the left and below the solid black line, while the grey dashed contours show the LSP mass. To the right of the red line, the reheating temperature lies above the freeze-out temperature and the resulting density is thermal. The colored dashed contours correspond to bounds from indirect detection for different DM density profiles, excluding everything below and to the right of them.[8] This figure also shows a funnel region with very low relic density along the $m_{\chi_1^0} = 500$ GeV contour corresponding to an s-channel A^0 pseudoscalar resonance.

In general, for $m_\varphi \sim m_{3/2}$, we find that a Higgsino-like LSP also tends to produce too much dark matter when it is created in moduli reheating. As for the wino, this can be avoided for larger values of $m_\varphi/m_{3/2}$, as demonstrated by Fig. 1, although one must still ensure that the very heavy modulus does not decay significantly to gravitinos.

These results can be extended to an arbitrary MSSM neutralino LSP. In general, mixing with a bino will further suppress the annihilation cross section, leading to an overproduction of dark matter for $m_\varphi \sim m_{3/2}$. The only loophole we can see is a very strong enhancement of the annihilation from a resonance or coannihilation [78]. This requires a very close mass degeneracy either between $2m_\chi$

[6]We have assumed radiation domination here, but a similar result holds for matter domination.

[7]We also fail to find any such points for $c = 100$ and $m_\varphi = 2m_{3/2}$.

[8]The details of our indirect detection analysis will be presented in the next section.

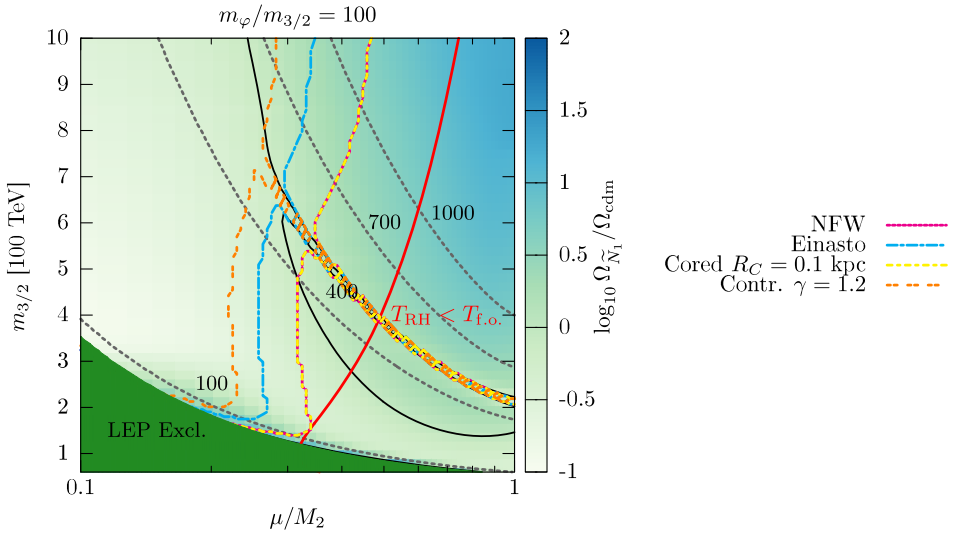

FIG. 1 (color online). Relic density and constraints from indirect detection (ID) for a mixed Higgsino-wino LSP produced by moduli reheating as a function of μ/M_2 and $m_{3/2}$. The modulus parameters are taken to be $m_\varphi/m_{3/2} = 100$, $c = 1$, and $\mathcal{N}_\chi = 1$. Contours of the LSP mass in GeV are given by the dashed grey lines. The solid black contours show where $\Omega_{\chi_1^0} = \Omega_{\rm cdm}$. The solid red line shows where $T_{\rm RH} = T_{\rm fo}$: to the left of it we have $T_{\rm RH} > T_{\rm fo}$; to the right $T_{\rm RH} < T_{\rm fo}$ and the production is nonthermal. The remaining lines correspond to bounds from ID for different galactic DM distributions, and the area below and to the right of these lines is excluded.

and the mass of the resonant state, or between m_χ and the coannihilating state, with coannihilation further suppressed at low reheating temperatures. The only other viable LSP candidates in the MSSM are the sneutrinos. These annihilate about as efficiently as a Higgsino-like LSP [79], and therefore also tend to be overproduced. The MSSM sneutrinos also have a very large scattering cross section with nuclei, and bounds from direct detection permit them to be only a small fraction of the total DM density [80].

Having expanded slightly on the findings of Ref. [50], we conclude that a neutral MSSM LSP is typically overproduced in moduli reheating unless $m_\varphi \gg m_{3/2}$ (with tiny $\mathrm{BR}_{3/2}$), $\mathcal{N}_\chi \ll 1$, or the decay coefficient $c \gg 100$ is very large. None of these features appears to be generic in string compactifications. We call this the *moduli-induced MSSM LSP problem*. For this reason, we turn next to extensions of the MSSM with more general LSP candidates that can potentially avoid this problem.

IV. VARIATION #1: HIDDEN $U(1)$

The first extension of the MSSM that we consider consists of a hidden $U(1)_x$ vector multiplet X and a pair of hidden chiral multiplets H and H' with charges $x_{H,H'} = \pm 1$. Motivated by the scaling relation of Eq. (16), we take the characteristic gauge coupling and mass scale of the hidden sector to be significantly less than electroweak, along the lines of Refs. [81–83]. The LSP of the extended theory will therefore be the lightest hidden neutralino. We also assume that the only low-energy interaction between the hidden and visible sectors is gauge kinetic mixing. Among other things, this allows the lightest MSSM superpartner to decay to the hidden sector. In this section we the investigate the contribution of the hidden LSP to the dark matter density following moduli reheating as well as the corresponding bounds from indirect and direct detection.

A. Setup and spectrum

The hidden superpotential is taken to be

$$W_{\rm HS} = W_{\rm MSSM} - \mu' H H', \tag{20}$$

and the soft supersymmetry-breaking terms are

$$-\mathcal{L}_{\rm soft} \supset m_H^2 |H|^2 + m_{H'}^2 |H'|^2 + \left(-b' H H' + \frac{1}{2} M_x \tilde{X}\tilde{X} + \text{H.c.}\right). \tag{21}$$

The only interaction with the MSSM comes from supersymmetric gauge kinetic mixing in the form

$$\mathcal{L} \supset \int d^2\theta \frac{\epsilon}{2} X^\alpha B_\alpha, \tag{22}$$

where X and B are the $U(1)_x$ and $U(1)_Y$ field strength superfields, respectively.

We assume that the gaugino mass is given by its AMSB value [82],

$$M_x = b_x \frac{g_x^2}{(4\pi)^2} m_{3/2}, \tag{23}$$

where $b_x = 2$ and g_x is the $U(1)_x$ gauge coupling. Since pure AMSB does not provide a viable scalar spectrum in the MSSM, we do not impose AMSB values on the scalar soft terms in the hidden sector. However, we do assume that they (and μ') are of similar magnitude to their AMSB values, on the order of $(g_x^2/16\pi^2)m_{3/2}$. This could arise if the dynamics that leads to a viable MSSM spectrum also operates in the hidden sector and its effects are proportional to the corresponding gauge coupling.

For a range of values of μ' and the soft terms, the scalar components of H and H' will develop vacuum expectation values,

$$\langle H\rangle = \eta \sin\zeta, \qquad \langle H'\rangle = \eta\cos\zeta. \tag{24}$$

Correspondingly, the hidden vector boson X_μ receives a mass

$$m_x = \sqrt{2} g_x \eta. \tag{25}$$

The scalar mass eigenstates after $U(1)_x$ breaking consist of two CP-even states $h^x_{1,2}$ (with h^x_1 the lighter of the two) and the CP-odd state A^x. The fermionic mass eigenstates are mixtures of the hidden Higgsinos and the $U(1)_x$ gaugino, and we label them in order of increasing mass as $\chi^x_{1,2,3}$. Full mass matrices for all these states can be found in Refs. [84,85].

B. Decays to and from the hidden sector

Kinetic mixing allows the lightest MSSM neutralino to decay to the hidden sector. It can also induce some of the hidden states to decay back to the SM. We discuss the relevant decay modes here.

The MSSM neutralinos connect to the hidden sector through the bino. For AMSB gaugino masses, the bino soft mass is significantly heavier than that of the wino, and the lightest neutralino χ^0_1 tends to be nearly pure wino. Even so, it will have a small bino admixture given by the mass mixing matrix element $\mathbf{N}_{11}$. In the wino limit, it can be approximated by [48]

$$|\mathbf{N}_{11}| = \frac{c_W s_W m_Z^2 (M_2 + \sin 2\beta\mu)}{(M_1 - M_2)(\mu^2 - M_2^2)}. \tag{26}$$

With this mixing, the lightest MSSM neutralino will decay to the hidden sector through the channels $\chi^0_1 \to \chi^x_k + S^x$, where χ^x_k are the hidden neutralinos and $S^x = h^x_{1,2}, A^x, X_\mu$ are the hidden bosons, with total width [84]

$$\begin{aligned}\Gamma_{\chi^0_1} &= \frac{\epsilon^2 g_x^2 |\mathbf{N}_{11}|^2}{4\pi} m_{\chi^0_1} \\ &= (1.3\times 10^{-16}\ \text{sec})^{-1} |\mathbf{N}_{11}|^2 \left(\frac{\epsilon}{10^{-4}}\right)^2 \left(\frac{g_x}{0.1}\right)^2 \\ &\quad\times \left(\frac{m_{\chi^0_1}}{100\ \text{GeV}}\right).\end{aligned} \tag{27}$$

The corresponding χ^0_1 lifetime should be less than about $\tau \lesssim 0.1$ s to avoid disrupting nucleosynthesis. This occurs readily for MSSM gaugino masses below the TeV scale and ϵ not too small.

In the hidden sector, the χ^x_1 neutralino will be stable while the other states will ultimately decay to it or to the SM. To ensure that χ^x_1 is able to annihilate efficiently, it should also be heavier than the vector X^μ. This implies that the hidden vector will decay to the SM through kinetic mixing, or via $X \to h^x_1 A^x$. For $m_x > 2m_e$, the vector decay width to the SM is

$$\Gamma(X \to \text{SM} + \text{SM}) = R' \frac{\alpha\epsilon^2 m_x}{3}, \tag{28}$$

where R' is a constant on the order of unity that depends on the number of available final states. This decay is much faster than $\tau = 0.1$ s for $\epsilon \gtrsim 4\times 10^{-10}$ and $m_x \gtrsim 2m_\mu$.

Of the remaining hidden states, the longest-lived is typically the lightest CP-even scalar h^x_1. The structure of the hidden sector mirrors that of the MSSM, and this scalar is always lighter than the vector at tree level. Loop corrections are not expected to change this at weak coupling. As a result, the h^x_1 decays exclusively to the SM through mixing with the MSSM Higgs scalars (via a Higgs portal coupling induced by gauge kinetic mixing) or through a vector loop [84]. This decay is typically faster than $\tau = 0.1$ s for $\epsilon \gtrsim 2\times 10^{-4}$ and $m_{h^x_1} \gtrsim 2m_\mu$ [85].

Light hidden sectors of this variety are strongly constrained by fixed-target and precision experiments [86,87]. For dominant vector decays to the SM, the strongest limits for $m_x > 2m_\mu$ come from the recent BaBar dark photon search [88], and limit $\epsilon \lesssim 5\times 10^{-4}$. As the vector mass approaches $m_x = 20$ MeV, fixed-target searches become relevant and constrain the mixing ϵ to extremely small values [86,87]. In this analysis, we will typically choose $m_x > 20$ MeV and $\epsilon \sim 10^{-4}$ so that the hidden sector is consistent with existing searches.

C. Hidden dark matter from moduli

Moduli decays are expected to produce both visible and hidden particles and reheat both sectors. The superpartners created by moduli decays will all eventually cascade down to the hidden neutralino LSP. Kinetic mixing can allow the hidden LSP to thermalize by scattering elastically with the SM background through the exchange of X vector bosons. The rate of kinetic equilibration depends on the typical energy at which the LSP is created, the reheating temperature, and the mass and couplings in the hidden sector [46]. For optimistic parameter values we find that it is faster than the Hubble rate for $T_{\text{RH}} \gtrsim 5$ MeV, and we will assume here that such thermalization occurs.

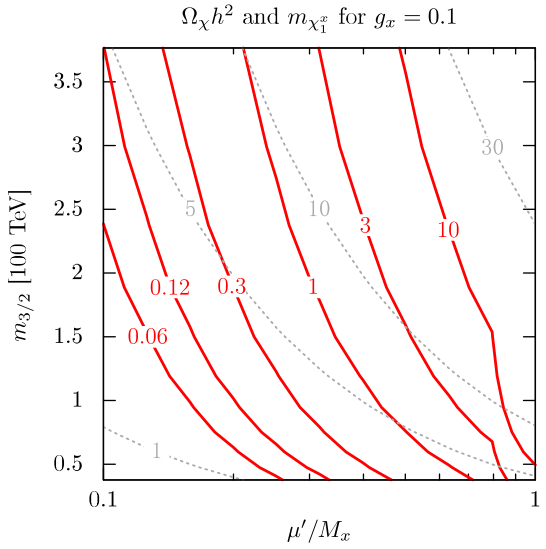

FIG. 2 (color online). Contours of the hidden neutralino χ_1^x mass in GeV (dashed grey) and moduli-generated relic abundance $\Omega_\chi h^2$ (solid red) as a function of μ'/M_x and $m_{3/2}$. The moduli parameters are taken to be $m_\varphi = m_{3/2}$, $c = 1$, and $\mathcal{N}_\chi = 1$, with the hidden-sector parameters as described in the text.

If the net rate of superpartner production in moduli decays is unsuppressed and the χ_1^x annihilation cross section is moderate, the χ_1^x LSPs will undergo additional annihilation to produce a final relic density as described in Eq. (10). The relevant annihilation modes of the LSP are $\chi_1^x\chi_1^x \to h_1^x h_1^x, Xh_1^x, XX$. Computing the corresponding annihilation rates using the method of Ref. [89] near $T \sim T_{\rm RH}$, we find that the XX final state typically dominates provided it is open, as we will assume here. Using these rates, we compute the relic abundance of χ_1^x by numerically solving the system of equations presented in Sec. II. In doing so, the decays of the MSSM LSP and all hidden states are treated as being prompt.

Before presenting our numerical results, it is instructive to examine the parametric dependence of the approximate solution of Eq. (10). Writing

$$\mu' = \xi M_x, \tag{29}$$

and focusing on a hidden Higgsino-like LSP with $\xi \leq 1$, we obtain $g_\chi = g_x$ and $r_\chi = 2\xi$ in Eq. (16). Thus, smaller values of ξ and g_x are expected to produce decreased χ_1^x relic abundances.

The results of a full numerical analysis are illustrated in Fig. 2, where we show the contours of the final χ_1^x abundance (solid red) and DM mass (dashed grey) in the $\xi - m_{3/2}$ plane for $m_\varphi = m_{3/2}$, $c = 1$, and $\mathcal{N}_\chi = 1$. The range of $m_{3/2}$ considered corresponds to $M_2 \in [100, 1000]$ GeV, and the hidden sector parameters are taken to be $g_x = 0.1$, $\tan\zeta = 10$, and $m_x = 0.2$ GeV, $m_{A^x} = 10$ GeV. The shape of the abundance contours in Fig. 2 is in agreement with the scaling predicted by Eq. (16). We also see that $\xi = \mu'/M_x < 1$ is typically needed to avoid creating too much dark matter, and this implies some degree of fine tuning for hidden-sector symmetry breaking. Larger values of ξ are allowed when the moduli decay parameter c is greater than unity, since this leads to a higher reheating temperature and more efficient reannihilation.

D. Constraints from indirect detection

While this extension of the MSSM can yield an acceptable hidden neutralino relic density from moduli reheating, it is also constrained by indirect detection (ID) searches for DM.[9] The pair annihilation of hidden neutralinos can produce continuum photons at tree level from cascades induced by $\chi_1^x\chi_1^x \to XX$ with $X \to f\bar{f}$, as well as photon lines at loop level through kinetic mixing with the photon and the Z^0. These signals have been searched for by a number of gamma ray telescopes, and limits have been placed on the corresponding gamma ray fluxes. We examine here the constraints on the χ_1^x state from observations of the Galactic center (GC) gamma ray continuum by the Fermi Large Area Telescope (Fermi-LAT) [90], as well as from observations of the diffuse photon flux by the INTEGRAL [91], COMPTEL [92], EGRET [93], and Fermi [94] experiments. For the GeV-scale dark matter masses we are considering, these observations are expected to give the strongest constraints [95,96].[10] We also study bounds from the effects of DM annihilation during recombination on the cosmic microwave background (CMB) [97,98].

The continuum photon flux from χ_1^x pair annihilation into hidden vectors is given by

$$\frac{d\Phi_\gamma}{dE_\gamma} = \frac{\langle\sigma v\rangle_{\chi\chi\to XX}}{8\pi m_\chi^2}\frac{dN_\gamma^{\rm tot}}{dE_\gamma} \times \int dl\rho^2(l), \tag{30}$$

where $\langle\sigma v\rangle_{\chi\chi\to XX}$ is the thermally averaged annihilation rate at present, $\rho(l)$ is the dark matter density along the line of sight l, and $dN_\gamma^{\rm tot}/dE_\gamma$ is the total differential photon yield per annihilation, defined as

$$\frac{dN_\gamma^{\rm tot}}{dE_\gamma} \equiv \sum_f {\rm BR}_f \frac{dN_\gamma^f}{dE_\gamma}, \tag{31}$$

where ${\rm BR}_f$ is the branching fraction of the XX state into the final state f.

[9]Constraints from direct detection are not relevant; the χ_1^x LSP is a Majorana fermion and scatters off nuclei mainly through a suppressed Higgs mixing coupling [85].

[10]We have also examined constraints from monochromatic photon line searches and found the continuum constraints significantly more stringent for the small values of ϵ allowed by fixed target experiments.

In our calculations, we use the results of Refs. [99,100] to estimate the partial yields dN_γ^f/dE_γ by interpolating between the results for the values of m_χ and m_χ/m_x listed in these studies. For the dark matter density profile, we consider four distributions that span the range of reasonable possibilities: Navarro-Frenk-White (NFW) [101], Einasto [102,103], contracted [95], and cored NFW [95]. These take the forms

$$\rho(r) \propto \begin{cases} \left[\frac{r}{R_s}\left(1+\frac{r}{R_s}\right)^2\right]^{-1} & \text{(NFW)} \\ e^{-2/\alpha\left[\left(\frac{r}{R_s}\right)^\alpha - 1\right]} & \text{(Einasto)} \\ \left[\left(\frac{r}{R_s}\right)^\gamma \left(1+\frac{r}{R_s}\right)^{3-\gamma}\right]^{-1} & \text{(contracted)} \\ \left[\frac{r_c+(r-r_c)\Theta(r-r_c)}{R_s}\left(1+\frac{r_c+(r-r_c)\Theta(r-r_c)}{R_s}\right)^2\right]^{-1} & \text{(cored)} \end{cases}. \tag{32}$$

Here, r is the radial distance from the GC and Θ is a step function. Following Refs. [50,95], we fix the scale radius to be $R_s = 20$ kpc and the Einasto parameter $\alpha = 0.17$. For the contracted profile we set $\gamma = 1.4$ and for the cored profile we set the core radius to be $r_c = 1$ kpc, as in Ref. [95]. In all four cases, we fix the overall normalization such that $\rho(r = 8.5\ \text{kpc}) = 0.3\ \text{GeV/cm}^3$.

Using these halo profiles, we are able to compute the gamma ray fluxes from hidden dark matter created in moduli decays and compare them to limits derived from observations of the GC and the diffuse gamma ray background. For the GC signal, we use the limits on $\langle\sigma v\rangle/m_\chi^2 \int_{E_{\rm min}}^{E_{\rm max}} dE_\gamma dN_\gamma^{\rm tot}/dE_\gamma$ computed in Ref. [95] in several energy bins $[E_{{\rm min},i}, E_{{\rm max},i}]$ and each of the four DM profiles described above. For the diffuse gamma ray background, we use the flux limits compiled and computed in Ref. [96].

In addition to measurements of cosmic gamma rays, observations of the CMB also provide a significant limit on DM annihilation [97,98]. The energy released by dark matter annihilation around the time of recombination will distort the last scattering surface, and hence affect the CMB anisotropies. The limit derived from this effect is [104–106]

$$f\frac{\Omega_\chi^2}{\Omega_{\rm cdm}^2}\langle\sigma v\rangle_{\rm CMB} \leq (2.42\times 10^{-27}\ \text{cm}^3/\text{s})\left(\frac{m_\chi}{\text{GeV}}\right), \tag{33}$$

where $\langle\sigma v\rangle_{\rm CMB}$ is the thermally averaged cross section during recombination and f is a constant efficiency factor parametrizing the fraction of energy transferred to the photon-baryon fluid, which can typically range from $f \approx 0.2$–1.0 [106]. We will vary f across this range to illustrate its effect on the resulting constraint.

These observations put very strong constraints on hidden dark matter when it is produced in moduli decays. The corresponding ID and CMB bounds are shown in Fig. 3 in the $m_{3/2} - g_x$ plane. We fix the moduli parameters to $m_\varphi = m_{3/2}$ and $c = 1$ in the left panel and $m_\varphi = 2m_{3/2}$ and $c = 10$ in the right. The relevant hidden-sector parameters are taken to be $\xi = 0.1$ and $m_x = m_\chi/2$. The solid red line shows where $\Omega_\chi = \Omega_{\rm cdm}$, with the region above and to the right of the line producing too much dark matter. The green shaded regions show the exclusion from Fermi observations of the GC assuming the Einasto DM profile of Eq. (32) rescaled by the expected dark matter fraction $(\Omega_\chi/\Omega_{\rm cdm})^2$, while the blue shaded regions show the exclusion from COMPTEL under the same conditions. Exclusions for other profiles are also shown by the parallel contours.[11] We have also considered the corresponding constraints from INTEGRAL, EGRET, and Fermi diffuse gamma ray observations, but these do not exclude any additional parameter space and so are not included in Fig. 3 for clarity. Limits from CMB distortions are shown by the solid and dash-dotted orange lines, for $f = 0.2$ and 1, respectively, with the excluded region above and to the right of the contours. The dashed black lines are contours of the hidden LSP χ mass in GeV, with the region where $m_x = m_\chi/2 < 20$ MeV excluded by fixed target experiments [86].

For generic moduli parameters, $c = 1$ and $m_\varphi = m_{3/2}$, we find that constraints from indirect detection and CMB observations nearly completely rule out this scenario even with optimistic choices for the DM halo properties and CMB energy injection efficiency. However, for $c = 10$ and $m_\varphi = 2m_{3/2}$, the hidden neutralino relic density can become sufficiently small to evade the strong limits from ID and the CMB, despite the relatively large χ_1^x annihilation cross section. In this case, a second more abundant contribution to the total dark matter abundance would be needed. Note as well that the remaining allowed region corresponds to sub-GeV hidden sector masses that could potentially be probed in current and planned precision searches [87].

E. Summary

With optimistic but reasonable choices for the moduli parameters, a light hidden sector neutralino LSP produced in moduli reheating can be consistent with current DM

[11] The thick green and blue dashed lines show the boundaries of the regions excluded for a more aggressive contracted profile with $\gamma = 1.4$. For clarity, we do not shade the interior of these. The thick solid and thin dotted contours correspond to the NFW and cored profiles, respectively.

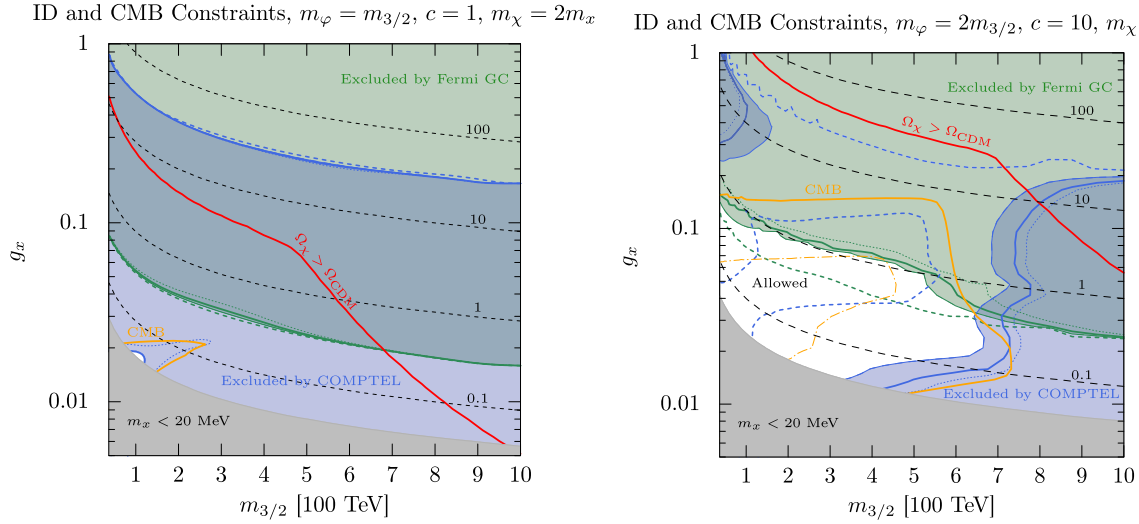

FIG. 3 (color online). Constraints from indirect detection on hidden $U(1)_x$ neutralino DM produced by moduli decays for $m_x = m_\chi/2$, $\xi = 0.1$, as well as $(c = 1, m_\varphi = m_{3/2})$ (left), and $(c = 10, m_\varphi = 2m_{3/2})$ (right). The green shaded region is excluded by Fermi GC observations and the blue shaded region is excluded by COMPTEL. Both exclusions assume an Einasto galactic DM profile. The thick solid and thin dotted contours correspond to the exclusions assuming the NFW and cored profiles, respectively. The green and blue dashed lines show the boundaries of the stronger exclusion obtained assuming a contracted profile with $\gamma = 1.4$. Above and to the right of the solid red line, the hidden LSP density is larger than the observed DM density. The solid and dash-dotted orange lines shows the exclusion from deviations in the CMB for $f = 0.2$ and $f = 1$, respectively, with the excluded areas above and to the right of the lines. Note that the entire $c = 1$ parameter space is excluded by the CMB constraint for $f = 1$. The gray shaded region at the bottom has a hidden vector mass $m_x < 20$ MeV that is excluded by fixed-target experiments.

searches. Even so, the scenario is tightly constrained by indirect detection and CMB measurements. The challenge here is precisely the same as in the MSSM: to avoid overproducing the neutralino LSP during moduli reheating, the annihilation rate must be large relative to the standard thermal value $\langle\sigma v\rangle \sim 3 \times 10^{-26}$ cm^3/s, and such an enhanced rate is strongly constrained by indirect DM searches. To avoid these bounds while not creating too much dark matter, the annihilation rate must be large enough that the LSP relic abundance is only a small fraction of the total DM density.

The $U(1)_x$ hidden sector does slightly better than the MSSM in this regard for two reasons. First, the hidden gauge coupling can be taken small (as can $\xi = \mu'/M_x$), which helps to reduce the LSP relic abundance as suggested by Eq. (16). And second, the hidden LSP can be much lighter than an MSSM wino or Higgsino, leading to smaller photon yields below the primary sensitivity of Fermi-LAT. The strongest constraints for such light masses come from COMPTEL, which are less stringent than those from Fermi. Since the large late-time hidden neutralino annihilation rate is the primary hindrance to realizing this setup, one might consider analogous scenarios in which the CMB and indirect detection signatures are suppressed; we address this possibility in the following section.

Before moving on, let us also comment on the spectrum in the hidden sector. To avoid a large fine tuning, the hidden scalar soft terms must be relatively small, on the same order or less than the hidden gaugino mass. Given the large values of $m_{3/2}$ considered, the scalar soft masses must be sequestered from supersymmetry breaking. They must also receive new contributions beyond minimal AMSB, and the b' bilinear soft term must not be too much larger than $(\mu')^2$. All three features require nontrivial additional structure in the underlying mechanisms of supersymmetry breaking or mediation [107,108].

V. VARIATION #2: ASYMMETRIC HIDDEN $U(1)$

As a second extension of the MSSM, we investigate a theory of hidden asymmetric dark matter (ADM) [109–112]. In the ADM framework, the DM particle has a distinct antiparticle, and its abundance is set mainly by a particle-antiparticle asymmetry in analogy to baryons, and this tends to suppress indirect detection signals from late-time annihilation if very little anti-DM is present [113–116]. The ADM theory we consider is nearly identical to the hidden $U(1)_x$ theory studied in Sec. IV, but with an additional pair of vectorlike hidden chiral superfields Y and Y^c with $U(1)_x$ charges $x_Y = \pm 1$. We assume that a small asymmetry in the Y density is generated during moduli reheating, in addition to the much larger symmetric density, and we compute the resulting relic densities and experimental signals.

A. Mass spectrum and decays

The superpotential in the hidden sector is same as that considered in Sec. IV up to a new mass term for the Y and Y^c multiplets,

$$W \supset -\mu_Y Y Y^c. \tag{34}$$

We also include the new soft supersymmetry-breaking terms

$$-\mathcal{L}_{\rm soft} \supset m_{\tilde{Y}}^2 |\tilde{Y}|^2 + m_{\tilde{Y}^c}^2 |\tilde{Y}^c|^2 - (b_Y \tilde{Y}\tilde{Y}^c + \text{H.c.}). \tag{35}$$

As in Sec. IV, we fix the hidden gaugino mass to its AMSB value with $b_x = 2(1+1)$, accounting for the new superfields. We also do not impose minimal AMSB values for the scalar soft terms, but take them (as well as μ' and μ_Y) to be of similar size to the gaugino soft mass. Finally, we arrange parameters so that the hidden Higgs scalars develop expectation values and spontaneously break the $U(1)_x$.

The mass spectrum of the hidden sector follows the minimal model considered in Sec. IV, but now a new Dirac fermion Ψ of mass $m_\Psi = \mu_Y$ and two complex scalars $\Phi_{1,2}$. The scalar mass matrix in the $(\tilde{Y}, \tilde{Y}^{c*})$ basis is

$$\mathcal{M}_{\tilde{Y}}^2 = \begin{pmatrix} |\mu_Y|^2 + m_{\tilde{Y}}^2 - \tilde{\delta}_D & b_Y^* \\ b_Y & |\mu_Y|^2 + m_{\tilde{Y}^c}^2 + \tilde{\delta}_D, \end{pmatrix}, \tag{36}$$

where $\tilde{\delta}_D = g_x^2 \eta^2 \cos 2\zeta + x_Y \epsilon g_x g' v^2 \cos 2\beta/2$. Taking $m_{\tilde{Y}}^2 = m_{\tilde{Y}^c}^2$ for convenience, the mass eigenvalues are

$$m_{1,2}^2 = |\mu_Y|^2 + m_{\tilde{Y}}^2 \mp \sqrt{\tilde{\delta}_D^2 + |b_Y|^2}. \tag{37}$$

In what follows, we will refer to the lighter scalar Φ_1 as Φ.

This theory preserves both the usual R parity as well as a nonanomalous global $U(1)$ flavor symmetry among the Y and Y^c multiplets, and can support multiple stable states. The number of stable particles depends on the mass spectrum. To allow for dominantly asymmetric dark matter, we will focus on spectra with $m_{\chi_1^x} > m_\Psi + m_\Phi$ such that the decay $\chi_1^x \to \Psi + \Phi^*$ is possible, and the only stable hidden states are Ψ and Φ. If this channel is not kinematically allowed, the χ_1^x neutralino will also be stable and can induce overly large gamma ray signals as in the previous section. We also choose soft masses such that $m_x < m_\Phi, m_\Psi$ to allow both states to annihilate efficiently into hidden vectors. With this mass ordering, the lightest hidden states will be the vector X^μ and the hidden Higgs h_1^x. Both will decay to the SM in the same way as in the minimal model of Sec. IV. The lightest MSSM neutralino will also continue to decay to the hidden sector through gauge kinetic mixing, now with additional decay modes $\chi_1^0 \to \Psi\Phi_{1,2}$. As before, the net χ_1^0 lifetime is expected to be short relative to the cosmological timescales of interest.

B. Moduli reheating and asymmetric dark matter

The Ψ and Φ states will both act as ADM if they are created in the moduli reheating process slightly more often than their antiparticles. The production of the asymmetry can be accommodated within a set of Boltzmann equations similar to Eq. (8) as follows:

$$\begin{aligned} \frac{dn_\Psi}{dt} + 3Hn_\Psi = (1+\kappa/2)\frac{\mathcal{N}_\Psi \Gamma_\varphi}{m_\varphi}\rho_\varphi \\ - \langle\sigma v\rangle_\Psi (n_\Psi n_{\bar{\Psi}} - (n_\Psi^{\rm eq})^2) \\ - \langle\sigma v\rangle_{\rm trans}(n_\Psi^2 - \nu^2 n_\Phi^2) \end{aligned} \tag{38}$$

$$\begin{aligned} \frac{dn_\Phi}{dt} + 3Hn_\Phi = (1+\kappa/2)\frac{\mathcal{N}_\Phi \Gamma_\varphi}{m_\varphi}\rho_\varphi \\ - \langle\sigma v\rangle_\Phi (n_\Phi n_{\Phi^*} - (n_\Phi^{\rm eq})^2) \\ - \langle\sigma v\rangle_{\rm trans}(\nu^2 n_\Phi^2 - n_\Psi^2), \end{aligned} \tag{39}$$

with a similar set of equations for the anti-DM $\bar{\Psi}$ and Φ^*, but with $\kappa \to -\kappa$. Here, $\mathcal{N}_\Psi$ and $\mathcal{N}_\Phi$ are the mean number of Ψ and Φ produced per modulus decay. This includes particles created directly in moduli decays, rescattering, and from the cascade decays of other states. The thermally averaged cross sections $\langle\sigma v\rangle_{\Psi,\Phi}$ describe the $\Psi\bar{\Psi}$ and $\Phi\Phi^*$ annihilation, while $\langle\sigma v\rangle_{\rm trans}$ in each equation corresponds to the transfer reaction $\Psi\Psi \leftrightarrow \Phi\Phi$ mediated by $U(1)_x$ gaugino exchange with $\nu = 2(m_\Psi/m_\Phi)^2 K_2(m_\Psi/T)/K_2(m_\Phi/T)$.

Asymmetry generation in this scenario is parametrized by the constant κ. It could arise directly from moduli decays or from the interactions of intermediate moduli decay products along the lines of one of the mechanisms of Refs. [117–123]. Indeed, this theory can be viewed as a simplified realization of the supersymmetric hylogenesis model studied in Ref. [124]. Relative to that work, we undertake a more detailed investigation of the relic density resulting from different choices for the moduli parameters, and we do not attempt to link the DM asymmetry to the baryon asymmetry.

The annihilation cross section $\langle\sigma v\rangle_\Psi$ is dominated by the $\Psi\bar{\Psi} \to XX$ channel to hidden vector bosons and is given by

$$\langle\sigma v\rangle_\Psi = \frac{1}{16\pi}\frac{g_x^4}{m_\Psi^2}\left(1 - \frac{m_x^2}{m_\Psi^2}\right)^{3/2}\left(1 - \frac{m_x^2}{2m_\Psi^2}\right)^{-2} \tag{40}$$

$$\simeq (1.5\times 10^{-24}\ \text{cm}^2/\text{s})\left(\frac{g_x}{0.05}\right)^4\left(\frac{1\ \text{GeV}}{m_\Psi}\right)^2. \tag{41}$$

The scalar annihilation rate is similar. For the transfer reaction, we have

$$\langle\sigma v\rangle_{\rm trans} \approx \frac{g_x^4}{8\pi}\sqrt{1 - \frac{m_\Phi^2}{m_\Psi^2}}\left|\sum_{k=1}^{3}\frac{(A_k^{*2} - B_k^2)m_{\chi_k^x}}{m_{\chi_k^x}^2 + m_\Psi^2 - m_\Phi^2}\right|^2, \tag{42}$$

where $A_k = \mathbf{Z}_{11}^* \mathbf{P}_{k3}$ and $B_k = \mathbf{Z}_{12}\mathbf{P}_{k3}$ with $\mathbf{P}_{k3}$ the HS gaugino content of χ_k^x and $\mathbf{Z}_{ij}$ the unitary matrix that diagonalizes the scalar mass matrix of Eq. (36). Note that the transfer reaction can be suppressed relative to annihilation for $m_{\chi_1^x} > m_\Psi + m_\Phi$.

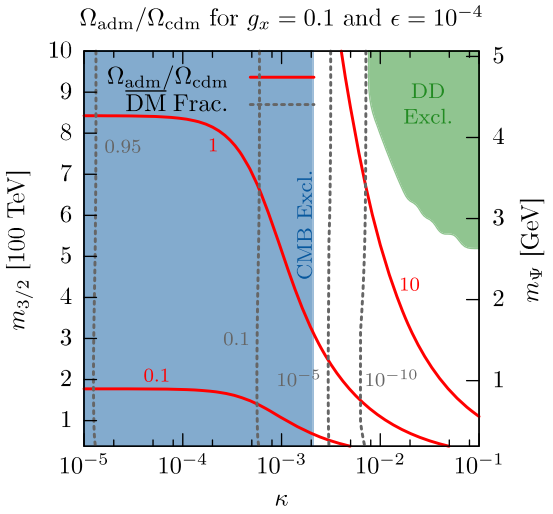

FIG. 4 (color online). Abundance of Ψ and Φ in the $\kappa - m_{3/2}$ plane. The right y axis shows the Ψ mass $m_\Psi = \mu_Y$. Solid red contours show the fraction of the measured abundance made up by Ψ and Φ and their antiparticles. The dashed grey lines show the fractional asymmetry between DM and anti-DM. The blue region is excluded by the CMB bound and the green by direct detection.

C. Relic densities and constraints

To investigate the relic densities of Ψ and Φ in this theory following moduli reheating and the corresponding constraints upon them, we set all the dimensionful hidden parameters to be fixed ratios of the $U(1)_x$ gaugino soft mass $M_x = 4g_x^2 m_{3/2}/(4\pi)^2$:

$$m_{A^x} = 10\mu' = 50\mu_Y = 100 m_x = 250 b_Y^{1/2} = 250 m_{\tilde{Y}} = M_x. \tag{43}$$

With these choices, the mass spectrum for $g_x = 0.1$ and $m_{3/2} = 200$ TeV is

$$m_\Psi = 1, \qquad m_\Phi = 0.97, \qquad m_{\chi_1^x} = 5.1,$$
$$m_x = 0.51, \qquad m_{h_1^x} = 0.5 \text{ GeV}.$$

This mass ordering coincides with the spectrum described in Sec. V A.

In Fig. 4 we show the dark matter abundance $\Omega_{\rm adm} = \rho_{\rm adm}/\rho_c$ of Ψ and Φ (and their antiparticles) relative to the observed abundance $\Omega_{\rm cdm}$ in the $\kappa - m_{3/2}$ plane for $g_x = 0.1$, $\epsilon = 10^{-4}$, $m_\varphi = m_{3/2}$, and $c = 1$. Contours of $\Omega_{\rm adm}/\Omega_{\rm cdm} = 0.1, 1, 10$ are given by solid red lines. The grey dashed lines in this figure correspond to the net residual anti-DM abundance $R_\Phi + R_\Phi$, where $R_\Psi = \Omega_{\bar\Psi}/\Omega_\Psi$ and similarly for Φ. Not surprisingly, larger values of the production asymmetry parameter κ lead to smaller residual anti-DM abundances. In this figure we also show in blue the region of parameters that is excluded by CMB observations, as well as the region excluded by direct detection in green. These constraints will be discussed in more detail below.

The ADM abundance in the $g_x - m_{3/2}$ plane is shown in Fig. 5 for $\kappa = 5 \times 10^{-3}$, $\epsilon = 10^{-4}$, $m_\varphi = m_{3/2}$, and $c = 1$. Again, contours of $\Omega_{\rm adm}/\Omega_{\rm cdm} = 0.1, 1, 10$ are given by solid red lines. We also plot contours of the Ψ mass with dashed grey lines. As before, the shaded green region is excluded by direct detection searches.

The region excluded by CMB observations in Fig. 4 (shaded blue) coincides with larger values of the residual anti-DM abundances $R_\Psi + R_\Phi$. These residual abundances provide an annihilation mode that injects energy into the cosmological plasma during the CMB era [115], as discussed in Sec. IV D. Accounting for exclusively asymmetric annihilation and the multiple DM species, the result of Eq. (33) translates into

$$2f \sum_{i=\Psi,\Phi} \left(\frac{\Omega_i + \Omega_{\bar i}}{\Omega_{\rm cdm}}\right)^2 \frac{R_i}{(1+R_i)^2} \frac{\langle\sigma v\rangle_i}{m_i} < \frac{2.42 \times 10^{-27}\ \text{cm}^3/\text{s}}{\text{GeV}}. \tag{44}$$

The CMB exclusion shown in Fig. 4 uses $f = 1$, but other values in the range $f = 0.2$–1.0 yield similar results. The boundary of the excluded region is also nearly vertical and independent of $m_{3/2}$. This can be understood in terms of an approximate cancellation of factors of $m_{3/2} = m_\varphi$ in the combination $\Omega_{\rm adm}^2 \langle\sigma v\rangle/m$, while R_i is determined primarily by κ. In addition to the limits from the CMB, we have also computed the bounds from indirect detection as described in Sec. IV. These searches yield exclusions very similar to that from the CMB and are omitted from Fig. 4.

Direct detection searches also place a significant constraint on this ADM scenario. Kinetic mixing of the hidden $U(1)_x$ with hypercharge links the hidden vector to charged matter with an effective coupling proportional to $-e\epsilon c_W$. In the present case, the dark matter consists of Dirac fermions and complex scalars charged under $U(1)_x$, and this allows a vectorial coupling of these states to the X gauge boson. Together, these two features induce a vector-vector effective operator (for $m_x \gtrsim 20$ MeV) connecting the DM states to the proton that gives rise to spin-independent (SI) scattering on nuclei. The Ψ-proton scattering cross section is

$$\sigma_p = \frac{\epsilon^2 c_W^2 e^2 g_x^2 \mu_n^2}{\pi m_x^4}. \tag{45}$$

A similar expression applies to the scalar Φ. This gives rise to an effective SI cross section per nucleon (in terms of which experimental limits are typically quoted) of

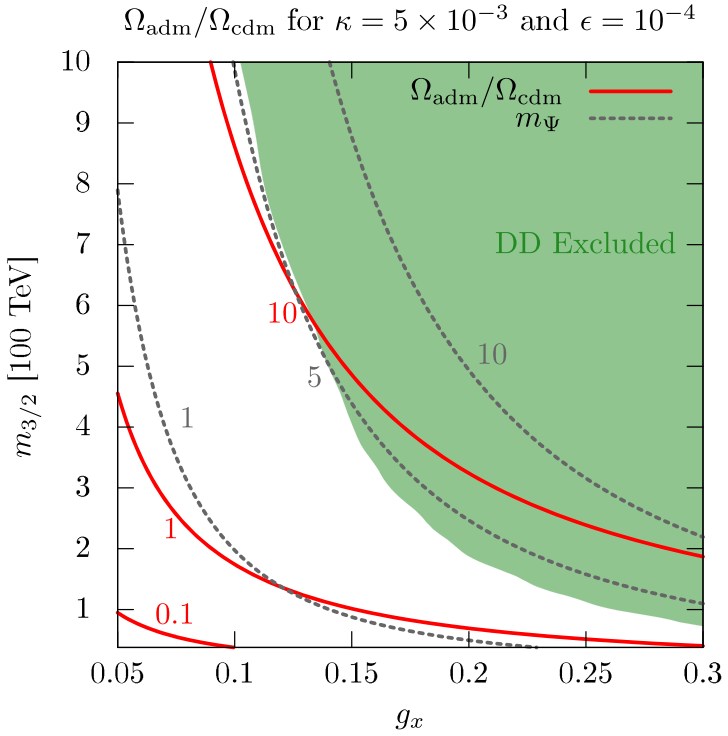

FIG. 5 (color online). Abundance of Ψ and Φ in the $g_x - m_{3/2}$ plane. Solid red contours show the fraction of the measured abundance made up by Ψ and Φ and their antiparticles. The dashed grey lines show the Ψ mass in GeV. The green region is excluded by direct detection.

$$\tilde{\sigma}_n = (Z^2/A^2)\sigma_p \simeq 2\times10^{-38}\ \text{cm}^2\left(\frac{2Z}{A}\right)^2\left(\frac{\epsilon}{10^{-3}}\right)^2\left(\frac{g_x}{0.1}\right)^2 \times\left(\frac{\mu_n}{1\ \text{GeV}}\right)^2\left(\frac{1\ \text{GeV}}{m_x}\right)^4. \quad (46)$$

Comparing this result to the exclusions of low-mass DM from LUX [125], XENON10 S2 only analysis [126], CDMSLite [127] and CRESST-Si [128], we obtain the green exclusion regions shown in Figs. 4 and 5.

D. Summary

This hidden $U(1)_x$ extension of the MSSM can account for the entire relic dark matter abundance in the aftermath of moduli reheating while being consistent with existing constraints from direct and indirect detection. Even though the DM annihilation cross section is much larger than the standard thermal value, a strong DM– anti-DM asymmetry allows for a significant total density while suppressing DM annihilation signals at late times. Limits from direct detection searches can also be evaded for light DM masses below the sensitivity of current experiments.

To achieve a strong DM asymmetry, a relatively large asymmetry parameter $\kappa \gtrsim 10^{-3}$ is needed. We have not specified the dynamics that gives rise to the asymmetry in moduli reheating, but more complete theories of asymmetry generation suggest that values this large can be challenging to obtain [118–120,124]. Furthermore, as in the symmetric hidden sector theory considered previously, the spectrum required for this mechanism to work requires scalar sequestering and scalar soft masses of the right size.

VI. VARIATION #3: HIDDEN $SU(N)$

The third extension of the MSSM that we consider consists of a pure supersymmetric $SU(N)_x$ gauge theory together with heavy connector matter multiplets charged under both $SU(N)_x$ and the MSSM gauge groups.[12] In contrast to the two previous extensions, we do not have to make any strong assumptions about the scalar soft mass parameters for the theory to produce an acceptable LSP relic density. In particular, this extension can work in the context of a *mini-split* spectrum where the scalar superpartners are much heavier than the gauginos [38–43].

A. $SU(N)_x$ mass spectrum and confinement

The hidden states below the TeV scale consist of the $SU(N)_x$ gluon and gluino. The hidden gluino soft mass is

$$M_x = r_x\frac{g_x^2}{(4\pi)^2}m_{3/2}, \quad (47)$$

[12]See also Refs. [129,130] for previous studies of this scenario in a slightly different context.

where $r_x = 3N$ if it is generated mainly by AMSB effects. In the discussion to follow, we will consider additional heavy matter charged under $SU(N)_x$ with large supersymmetric mass μ_F. For $\mu_F \gg m_{3/2}$, the coefficient r_x will be unchanged [26]. However, when $\mu_F \lesssim m_{3/2}$, the value of r_x can be modified by an amount of order unity that depends on the soft masses of these states [30,75]. We consider deviations in r_x away from the AMSB value but still of the same general size.

Below the hidden gluino mass, the hidden sector is a pure $SU(N)_x$ gauge theory. It is therefore guaranteed to be asymptotically free, and the low-energy theory of hidden gluons should undergo a confining transition at some energy scale Λ_x to a theory of massive glueball (and glueballino) bound states. The one-loop estimate of the confinement scale gives

$$\Lambda_x = M_x \exp\left(-\frac{3r_x}{22N}\frac{m_{3/2}}{M_x}\right). \tag{48}$$

Demanding that the $SU(N)_x$ gluino be lighter than the lightest MSSM neutralino typically forces Λ_x to be very small. For example, setting $M_x < 1000$ GeV, $r_x = 3N$, and requiring that $M_x < M_2$ (with its value as in AMSB, $M_2 \simeq m_{3/2}/360$), one obtains $\Lambda_x < 10^{-61}$ GeV. Thus, we will neglect $SU(N)_x$ confinement in our analysis and treat the hidden gauge theory as weakly interacting.

B. Connectors to the MSSM

The lightest MSSM superpartner must be able to decay to the hidden sector for this extension to solve the MSSM moduli relic problem. Such decays can be induced by heavy matter multiplets charged under both the MSSM gauge groups and $SU(N)_x$. Following Ref. [129], we examine two type of connectors.

The first set of connectors consists of N_F pairs of chiral superfields F and F^c with charges $(1, 2, \mp 1/2; N)$ under $SU(3)_c \times SU(2)_L \times U(1)_Y \times SU(N)_x$ with a supersymmetric mass term [129]

$$W \supset \mu_F F F^c. \tag{49}$$

For $\mu_F \gtrsim m_{3/2}$, the heavy multiplets can be integrated out supersymmetrically to give [129]

$$-\Delta\mathcal{L} \supset \int d^4\theta \frac{g_x^2 g_2^2}{(4\pi)^2}\frac{2N_F}{\mu_F^4} W^\dagger_{x\dot\alpha} W^{\dagger\dot\alpha} W^\alpha_x W_\alpha \tag{50}$$

$$\supset \alpha_x \alpha_2 \frac{2N_F}{\mu_F^4}[\tilde G_x^\dagger(\bar\sigma\cdot\partial)\tilde W G_x^{\mu\nu} W_{\mu\nu} + (G_x^{\mu\nu} W_{\mu\nu})^2]. \tag{51}$$

Similar operators involving the $U(1)_Y$ vector multiplet will also be generated, and additional operators will also arise with the inclusion of supersymmetry breaking. The wino operator of Eq. (51) allows the decay $\tilde W^0 \to W^0 G_x \tilde G_x$, whose rate we estimate to be

$$\begin{aligned}\Gamma &\sim \frac{4(N^2-1)N_F^2}{8\pi(4\pi)^2}\alpha_x^2\alpha_2^2|\mathbf{N}_{12}|^2\frac{m_{\chi_1^0}^9}{\mu_F^8} \\ &\simeq (7\times 10^5\ \text{s})^{-1}(N^2-1)N_F^2|\mathbf{N}_{12}|^2\left(\frac{\alpha_x}{10^{-3}}\right)^2 \\ &\quad\times\left(\frac{m_{\chi_1^0}}{270\ \text{GeV}}\right)^9\left(\frac{100\ \text{TeV}}{\mu_F}\right)^8,\end{aligned} \tag{52}$$

where $m_{\chi_1^0}$ is the mass of the lightest MSSM neutralino, $|\mathbf{N}_{12}|$ is its wino content, and the fiducial value of $m_{\chi_1^0}$ corresponds to the AMSB value of M_2 for $m_{3/2} \simeq$ 100 TeV. Note that these sample parameter values lead to decays after the onset of primordial nucleosynthesis.

The second set of connectors that we consider consists of the same N_F heavy multiplets F and F^c together with P and P^c multiplets with charges $(1, 1, 0, \bar N)$ [129]. This allows the couplings

$$W \supset \lambda_u H_u F P + \lambda_d H_d F^c P^c + \mu_F F F^c + \mu_P P P^c. \tag{53}$$

Neglecting supersymmetry breaking, integrating out the heavy F and P multiplets at one-loop order generates operators such as [129]

$$-\Delta\mathcal{L} \supset \int d^2\theta \frac{g_x^2\lambda_u^2}{(4\pi)^2}\frac{2N_F}{\mu_F^2} W^{x\alpha} W_{x\dot\alpha} H_u\cdot H_d \tag{54}$$

$$\supset \alpha_x\left(\frac{\lambda_u^2}{4\pi}\right)\frac{2N_F}{\mu_F^2}[\tilde G_x\sigma_\mu\bar\sigma_\nu\tilde H_d H_u G_x^{\mu\nu} + G_x^{\mu\nu} G_{x\mu\nu} H_u\cdot H_d], \tag{55}$$

where we have set $\mu_P = \mu_F$ and $\lambda_d = \lambda_u$ for simplicity. Additional related operators arise when supersymmetry breaking is included. The first term in Eq. (55) induces the decay $\chi_1^0 \to G_x\tilde G_x$, whose rate we estimate to be

$$\begin{aligned}\Gamma &\sim \frac{4(N^2-1)N_F^2}{8\pi}\alpha_x^2\left(\frac{\lambda_u^2}{4\pi}\right)^2|\mathbf{N}_{13}|^2\frac{v_u^2 m_{\chi_1^0}^3}{\mu_F^4} \\ &\simeq (1\times 10^{-6}\ \text{s})^{-1}(N^2-1)N_F^2|\mathbf{N}_{13}|^2\left(\frac{\alpha_x}{10^{-3}}\right)^2\left(\frac{\lambda_u}{0.75}\right)^4 \\ &\quad\times\left(\frac{m_{\chi_1^0}}{200\ \text{GeV}}\right)^3\left(\frac{100\ \text{TeV}}{\mu_F}\right)^4,\end{aligned} \tag{56}$$

where $|\mathbf{N}_{13}|$ describes the $\tilde H_d$ content of the MSSM LSP. This decay can occur before primordial nucleosynthesis, even for very large values of $\mu_F \gtrsim 100$ TeV.

Finally, let us mention that the exotic doublets F and F^c will disrupt standard gauge unification. This can be restored by embedding these multiplets in **5** and $\bar{\mathbf{5}}$

representations of $SU(5)$ and limiting the amount of new matter to maintain perturbativity up to the unification scale [129]. The latter requirement corresponds to $N \times N_F \leq 5$ for $\mu_F \sim 100$ TeV.

C. Moduli reheating and hidden dark matter

The treatment of dark matter production by moduli reheating in this scenario is slightly different from the situations studied previously. The key change is that the visible and hidden sectors are unlikely to reach kinetic equilibrium with one another after reheating for $\mu_{F,P} \gtrsim m_{3/2}$. As a result, it is necessary to keep track of the effective visible and hidden temperatures independently.

To estimate kinetic equilibration, let us focus on the wino operator of Eq. (51). This gives rise to $G_x\gamma \to G_x\gamma$ scattering with a net rate of $\Gamma \sim T^9/\mu_F^8$. Comparing to the Hubble rate, kinetic equilibration requires $T_{\rm eq} \gtrsim (\mu_F^8/M_{\rm Pl})^{1/7}$. On the other hand, the reheating temperature after moduli decay is on the order $T_{\rm RH} \sim (m_{3/2}^3/M_{\rm Pl})^{1/2}$. Thus, we see that $T_{\rm RH}$ is parametrically smaller than $T_{\rm eq}$ for $\mu_F \gtrsim m_{3/2}$. A similar argument applies to the Higgs interaction in the second term in Eq. (55).

The total modulus decay rate is the sum of partial rates into the visible and hidden sectors,

$$\Gamma_\varphi = \frac{c}{4\pi}\frac{m_\varphi^3}{M_{\rm Pl}^2} = \Gamma_v + \Gamma_x = \frac{c_x + c_v}{4\pi}\frac{m_\varphi^3}{M_{\rm Pl}^2}, \tag{57}$$

where c_x and c_v describe the relative hidden and visible decay fractions. Moduli decays will reheat both sectors independently, and self-interactions within each sector will lead to self-thermalization. The total radiation density is the sum of the two sectors, $\rho_R = \rho_v + \rho_x$. We will also define effective temperatures within each sector by

$$\rho_v = \frac{\pi^2}{30} g_* T^4, \tag{58}$$

$$\rho_x = \frac{\pi^2}{30} g_{*x} T_x^4, \tag{59}$$

where g_* and T refer to the visible sector and g_{*x} and T_x to the hidden. Since the hidden and visible sectors do not equilibrate with each other after reheating, entropy will be conserved independently in both sectors.

Just after reheating, we also have

$$\rho_v = \left(\frac{c_v}{c}\right)\rho_R, \qquad \rho_x = \left(\frac{c_x}{c}\right)\rho_R. \tag{60}$$

Given the first equality, we now define the reheating temperature to be

$$T_{\rm RH} = \left(\frac{c_v}{c}\right)^{1/4}\left[\frac{90}{\pi^2 g_*(T_{\rm RH})}\right]^{1/4}\sqrt{\Gamma_\varphi M_{\rm Pl}}, \tag{61}$$

corresponding approximately to the visible radiation temperature when $H = \Gamma_\varphi$. In the same way, we also define the reheating temperature in the hidden sector to be $T_{\rm RH}^x = (c_x/c_v)^{1/4}(g_*/g_{*x})^{1/4} T_{\rm RH}$.

The number density of $SU(N)_x$ gaugino dark matter evolves according to Eq. (8) but with two important modifications. First, the quantity $\mathcal{N}_\chi$ now corresponds to the mean number of hidden gauginos produced per modulus decay. This includes production from direct decays, decay cascades (including decays of the lightest MSSM neutralino), and rescattering. The second key change is that the thermal average in $\langle\sigma v\rangle$ is now taken over the hidden-sector distribution with effective temperature $T_x \simeq T_{\rm RH}^x$.

The thermally averaged $SU(N)_x$ gaugino cross section can receive a nonperturbative Sommerfeld enhancement from multiple hidden gluon exchange if the hidden confinement scale is very low, as we expect here [131,132]. This enhancement can be written as a rescaling of the perturbative cross section,

$$\langle\sigma v\rangle = S_x \langle\sigma v\rangle_{\rm pert}. \tag{62}$$

The perturbative cross section can be obtained by modifying the $SU(3)_c$ gluino result [133] by the appropriate color factor:

$$\langle\sigma v\rangle_{\rm pert} = \frac{3N^2}{16(N^2-1)}\frac{1}{4\pi}\left(\frac{g_x^4}{M_x^2}\right). \tag{63}$$

The Sommerfeld enhancement factor is [131–133]

$$S_x = A/(1 - e^{-A}), \tag{64}$$

with $A = \pi\alpha_x/v$, for $v = \sqrt{1 - 4M_x^2/s}$. In the perturbative cross section, the characteristic momentum transfer is $\sqrt{s} \simeq 2M_x$, and α_x should be evaluated at this scale. However, the typical momentum transfer leading to the nonperturbative enhancement is $\sqrt{s} \sim 2vM_x$ [133]. In our calculation, we estimate $v \simeq \sqrt{3T_{\rm RH}^x/2M_x}$ and take A to be

$$A \simeq \frac{\pi}{2v}\alpha_x\left[1 + \frac{11N}{6\pi}\alpha_x \ln(v)\right]^{-1}, \tag{65}$$

where α_x in this expression is evaluated at $2M_x$.

In Fig. 6 we show the relic density of hidden gluinos produced by moduli reheating as a function of g_x for $m_\varphi = m_{3/2} = 100$ TeV, $c = 1$, $\mathcal{N}_\chi \sim 1$, and $c_x/c_v = 1/9$. We also show in this figure the lifetime of the lightest MSSM superpartner in seconds, which we take to be a Higgsino-like neutralino with $\mu = 150$ GeV, along with $N = 2$, $\mu_F = m_{3/2}$, $N_F = 3$, and $\lambda_u = 0.75$. As expected from the estimate of Eq. (16), smaller values of the gauge coupling $g_x \ll g_2$ are needed to obtain an acceptable relic density.

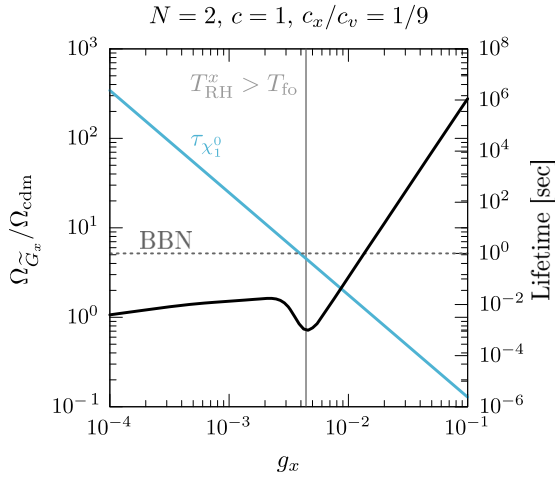

FIG. 6 (color online). Relic abundance of the hidden gluino $\tilde{G}_x$ (solid black) after moduli reheating as a function of the hidden gauge coupling g_x for $N = 2$, $m_\varphi = m_{3/2} = 100$ TeV, $c = 1$, $\mathcal{N}_x = 1$, and $c_x/c_v = 1/9$. The lifetime of the lightest MSSM superpartner, assumed to be a Higgsino-like neutralino, is shown in light blue for $\mu = 150$ GeV, $N_F = 3$, and $\lambda_u = 0.75$. The vertical solid grey line corresponds to $T^x_{\rm RH} \approx T_{\rm fo}$, while the dashed horizontal line shows $\tau_{\chi_1^0} = 1$ s.

For very small g_x, the hidden gluino mass becomes small enough that the reheating temperature exceeds the freeze-out temperature, and the final density is given by the thermal value. This corresponds to the plateau, where the abundance is only weakly dependent on the gauge coupling. At intermediate g_x, freeze-out happens in the matter dominated phase, where $\Omega_{\tilde{G}_x} \propto M_x^{-3} \propto g_x^{-6}$ [68], resulting in the turn-over. The abundance continues to decrease until nonthermal production takes over, corresponding to the straight section for $g_x \gtrsim 4 \times 10^{-3}$. Note as well that very small values of g_x also increase the lifetime of the lightest MSSM state to $\tau > 1$ s. This can be problematic for nucleosynthesis, and will be discussed in more detail below.

D. Hidden Gluino Bounds

We found previously that for $M_x < M_2$ and AMSB-like masses, the $SU(N)_x$ confinement scale is negligibly small relative to the Hubble scale today. This implies that the hidden gluon will be a new relativistic degree of freedom in the early Universe. A nearly massless hidden gluon will also interact significantly with the relic hidden gluinos, which has significant implications for dark matter clustering and its imprint on the CMB.

New relativistic particles are constrained by primordial nucleosynthesis and the CMB. The number of corresponding degrees of freedom is often written in terms of an effective number of additional neutrino species, $\Delta N_{\rm eff}$. If the hidden gluon is the only new light state below the reheating temperature and 5 MeV $< T_{\rm RH} < m_\mu$, we have [83]

$$\Delta N_{\rm eff} \simeq \left(\frac{4}{7}\right)(N^2 - 1)\left(\frac{c_x}{c_v}\right), \tag{66}$$

where c_x and c_v correspond to the hidden and visible branching fractions of the moduli. The current upper bound (95% c.l.) on $\Delta N_{\rm eff}$ from primordial nucleosynthesis is [134,135]

$$\Delta N_{\rm eff} \lesssim 1.0 \quad \text{at } T \sim T_{\rm BBN}. \tag{67}$$

This bound can be satisfied for smaller N provided $(c_x/c_v) < 1$. If we reinterpret our moduli results in terms of heavy gravitino decay, the corresponding ratio is $c_x/c_v = (N^2 - 1)/12$ if only gaugino modes are open and $c_x/c_v = 12(N^2 - 1)/193$ if all MSSM channels are available [69]. A similar limit on $N_{\rm eff}$ can be derived from the CMB [136]. However, the net effect of the hidden gluon and gluino on the CMB is more complicated than just a change in $\Delta N_{\rm eff}$, as we will discuss below.

A more significant challenge to this scenario comes from the relatively unsuppressed interactions among the hidden gluons and gluinos. Self-interactions among dark matter particles are strongly constrained by observations of elliptical galaxies and the Bullet Cluster [137–139].[13] Furthermore, we find that the relic hidden gluinos remain kinetically coupled to the hidden gluon bath until very late times. This generates a pressure in the dark gluino fluid that interferes with its gravitational collapse into bound structures. A study of this effect lies beyond the scope of this paper, and we only attempt to describe some of the general features here.

In this scenario, moduli reheating generates a bath of thermal gluons with temperature $T_x \sim (c_x/c_v)^{1/4} T$. Arising from a non-Abelian gauge group, the gluons will interact with themselves at the rate

$$\Gamma \sim \alpha_x^2 T_x \sim (10^{-12}\ \text{eV})\left(\frac{c_x}{c_v}\right)^{1/4}\left(\frac{\alpha_x}{10^{-4}}\right)^2\left(\frac{T}{2.7\ \text{K}}\right). \tag{68}$$

This is easily larger than the Hubble rate today, $H \sim 10^{-33}$ eV, and we expect the hidden gluon to remain in self-equilibrium at the present time. One of the key features of such non-Abelian plasmas at temperatures well above the confinement scale is that the gluon field is screened by its self-interactions [144,145]. Correspondingly, the electric and magnetic components of the gluon develop *Debye masses* on the order of [146],

$$m_E \sim \sqrt{\alpha_x} T_x \tag{69}$$

$$m_B \sim \alpha_x T_x. \tag{70}$$

[13]Dark matter interactions close to these upper bounds can help to resolve some of the puzzles of large-scale structure [130,140–143].

Relic hidden gluinos will interact with the hidden gluon bath through Compton-like scattering. This can proceed through a t-channel gluon with no suppression by the hidden gluino mass. Modifying the calculation of Refs. [147], we find that the corresponding rate of momentum transfer between a relic gluino and the gluon bath is much larger than the Hubble rate even at the present time. We also estimate that for moderate α_x and $m_\varphi \sim 100$ TeV the rate of formation of gluino-gluino bound states, which are expected to be hidden-color singlets in the ground state [148–150], is much smaller than the Hubble rate at temperatures below the binding energy.

Together, these two results imply that the relic gluinos remain kinetically coupled to the gluon bath. The pressure induced by the gluons will drive gluinos out of overdense regions and interfere with structure formation, analogous to the photon pressure felt by baryons before recombination. This is very different from the behavior of standard collisionless cold dark matter and implies the hidden gluinos can only be a small fraction of the total dark matter density. This fraction can be constrained using observations of the CMB and galaxy surveys. A study along these lines was performed in Ref. [151], and their results suggest that the fraction $f_x = \Omega_{\tilde{G}_x}/\Omega_{\rm cdm}$ must be less than a few percent, depending on the temperature ratio $T_x/T \simeq (c_x/c_v)^{1/4}$.[14] Hidden gluino interactions may also modify the distribution of dark matter on galactic scales [154].

E. Summary

This supersymmetric hidden $SU(N)_x$ extension can produce a much smaller nonthermal LSP relic density than the MSSM, and has only invisible annihilation modes that are not constrained by indirect detection. However, the hidden gluino LSP remains in thermal contact with a bath of hidden gluons, and thus can only make up at most a few percent of the total dark matter density. Obtaining such small relic densities is nontrivial and leads to new challenges, as we will discuss here.

From Fig. 6 we see that reducing the gauge coupling g_x lowers the nonthermal hidden gluino density until $T_{\rm RH} \sim T_{\rm fo}$, at which point the relic abundance becomes approximately constant in g_x. At the same time, Eq. (56) shows that smaller values of g_x also suppress the decay rate of the lightest MSSM superpartner. If such decays happen after the onset on primordial nucleosynthesis, they can disrupt the abundances of light elements [155,156]. The direct two-body decays $\chi_1^0 \to \tilde{G}_x G_x$ are invisible. However, the operator of Eq. (55) also gives rise to the semi-visible three-body mode $\chi_1^0 \to h^0 \tilde{G}_x G_x$ if it is kinematically allowed. The decay products of the Higgs boson will be significantly hadronic, and can modify light-element abundances. The branching fraction of this three-body mode depends on the available phase space. Taking it to be $B_h \sim 10^{-3}$ and estimating the Higgsino yield as in Sec. III, we find that Higgsino lifetimes below $\tau_{\chi_1^0} \lesssim 1$–$100$ s are allowed [155]. This can occur for larger values of N, N_F, or λ_u, or smaller values of μ or μ_F. Note that reducing μ_F below $m_\varphi/2$ is dangerous because it would lead to the production of stable massive F and P states which would tend to overclose the Universe.

An acceptable hidden gluino relic density with a sufficiently rapid MSSM decay can be obtained in this scenario, but only in a very restricted and optimistic region of parameters. For example, with $r_x = 3N/5$, $g_x = 0.01$, $N = 2$, $N_F = 3$, $\lambda_u = 0.75$, $c_x/c_v = 1/9$, and $m_\varphi = 2m_{3/2} = 2\mu_F = 100$ TeV, we obtain $\Omega_{\tilde{G}_x}/\Omega_{\rm cdm} = 0.023$ and $\tau_{\chi_1^0} = 0.01$ s. Compared to the parameters used in Fig. 6, the greatest effect comes from the small value of r_x relative to the minimal AMSB value ($r_x = 3N$). Such a reduction could arise from threshold corrections due to the heavy multiplets [75].

VII. CONCLUSIONS

In this work we have investigated the production of LSP dark matter in the wake of moduli oscillation and reheating. For seemingly generic string-motivated moduli parameters $m_\varphi = m_{3/2}$, $c = 1$, $\mathcal{N}_\chi \sim 1$, we have argued that the MSSM LSP is typically created with an abundance that is larger than the observed dark matter density. The exception to this is a winolike LSP, which has been shown to be inconsistent with current bounds from indirect detection. We call this the MSSM moduli-induced LSP problem.

To address this problem, we have studied three gauge extensions of the MSSM. In the first, the MSSM is expanded to include a lighter hidden $U(1)_x$ vector multiplet with kinetic mixing with hypercharge that is spontaneously broken by a pair of chiral hidden Higgs multiplets. The kinetic mixing interaction allows the lightest MSSM superpartner to decay to the lighter hidden sector LSP. If this LSP consists primarily of the hidden Higgsinos and is sufficiently light, it will annihilate very efficiently. The resulting hidden LSP relic abundance after moduli reheating can be small enough to be consistent with current bounds from indirect detection and the CMB. In this case, a second more abundant component of the DM density is needed. The spectrum of scalar soft terms required in this theory can also be challenging to obtain for the large values of $m_{3/2} \gtrsim 100$ TeV considered.

The second extension of the MSSM that we studied has an asymmetric dark matter candidate. The underlying theory in this case was again a kinetically mixed $U(1)_x$ vector multiplet spontaneously broken by a pair of chiral hidden Higgs, but now with an additional pair of chiral multiplets Y and Y^c. For a range of parameters, the two

[14] A relic population of millicharged particles will have a similar effect. This was considered in Refs. [152,153], and a limit of $f_x \lesssim 1\%$ was obtained.

stable states in this theory are the Dirac fermion Ψ and the lighter complex scalar Φ derived from Y and Y^c. If Ψ or Φ obtain a significant particle antiparticle asymmetry in the course of moduli reheating, they can account for the entire DM density. A large production asymmetry leads to a very small residual anti-DM component, which allows the asymmetric abundances of Ψ and Φ to be consistent with limits from indirect (and direct) detection. However, the production asymmetry required for this to work is relatively large, and may be difficult to obtain in a more complete theory of asymmetry generation. This theory also faces the same scalar soft term requirement as the symmetric hidden $U(1)_x$ extension.

The third extension of the MSSM consists of a pure non-Abelian $SU(N)_x$ vector multiplet at low energies. This sector can connect to the MSSM through additional heavy multiplets charged under both the visible and hidden gauge groups, allowing for decays of the lightest MSSM superpartner to the $SU(N)_x$ gluino. Acceptable hidden gluino relic densities can be obtained for smaller values of the $SU(N)_x$ gauge coupling. This implies a potential tension with primordial nucleosynthesis from late MSSM decays, and leads to a negligibly small hidden confinement scale. In contrast to the two previous extensions, light scalar superpartners are not required and this mechanism can work in the context of minisplit supersymmetry [38–43]. While this theory is not constrained by standard indirect detection searches, the coupling of the hidden gluino to a bath of hidden gluons leads to nonstandard DM dynamics that require the hidden gluino density to be only a few percent of the total DM density. It is very difficult to obtain relic densities this small in this scenario.

Our main conclusion is that it is challenging to avoid producing too much LSP dark matter in the course of string-motivated moduli reheating. For seemingly generic modulus parameters, the relic density in the MSSM is either too large or at odds with limits from indirect detection. This may be a hint that the properties of moduli (in our vacuum at least) differ from the general expectations discussed above [6,18]. Alternatively, this could be an indication of new light physics beyond the MSSM. We have considered three examples of the latter possibility in this paper and have shown that they can produce a stable LSP abundance that is consistent with current observations and limits. Even so, these three extensions all lead to a significant complication of the MSSM and require a somewhat fortuitous conspiracy of parameters for them to succeed. A more direct solution might be the absence of a stable LSP through R-parity violation or simply the absence of light superpartners and very large $m_\varphi \sim m_{3/2}$.

ACKNOWLEDGMENTS

We thank Matthew Reece, Kris Sigurdson, Scott Watson, and Kathryn Zurek for helpful discussions. This work is supported by the Natural Sciences and Engineering Research Council of Canada (NSERC).

[1] G. D. Coughlan, W. Fischler, E. W. Kolb, S. Raby, and G. G. Ross, Phys. Lett. **131B**, 59 (1983).
[2] J. R. Ellis, D. V. Nanopoulos, and M. Quiros, Phys. Lett. B **174**, 176 (1986).
[3] T. Banks, D. B. Kaplan, and A. E. Nelson, Phys. Rev. D **49**, 779 (1994).
[4] J. Polchinski, *String Theory. Vol. 1: An Introduction to the Bosonic String* (Cambridge University Press, Cambridge, England, 1998)
[5] J. Polchinski, *String Theory. Vol. 2: Superstring Theory and Beyond* (Cambridge University Press, Cambridge, England, 1998).
[6] B. S. Acharya, G. Kane, and P. Kumar, Int. J. Mod. Phys. A **27**, 1230012 (2012).
[7] B. de Carlos, J. A. Casas, F. Quevedo, and E. Roulet, Phys. Lett. B **318**, 447 (1993).
[8] F. Quevedo, Classical Quantum Gravity **19**, 5721 (2002).
[9] B. S. Acharya, P. Kumar, K. Bobkov, G. Kane, J. Shao, and S. Watson, J. High Energy Phys. 06 (2008) 064.
[10] M. Dine, L. Randall, and S. D. Thomas, Phys. Rev. Lett. **75**, 398 (1995).
[11] R. Durrer and J. Hasenkamp, Phys. Rev. D **84**, 064027 (2011).
[12] A. L. Erickcek and K. Sigurdson, Phys. Rev. D **84**, 083503 (2011).
[13] R. Easther, R. Galvez, O. Ozsoy, and S. Watson, Phys. Rev. D **89**, 023522 (2014).
[14] L. Iliesiu, D. J. E. Marsh, K. Moodley, and S. Watson, Phys. Rev. D **89**, 103513 (2014).
[15] J. J. Fan, O. Ozsoy, and S. Watson, Phys. Rev. D **90**, 043536 (2014).
[16] T. Moroi and L. Randall, Nucl. Phys. **B570**, 455 (2000).
[17] S. Hannestad, Phys. Rev. D **70**, 043506 (2004).
[18] M. Bose, M. Dine, and P. Draper, Phys. Rev. D **88**, 023533 (2013).
[19] S. Kachru, R. Kallosh, A. D. Linde, and S. P. Trivedi, Phys. Rev. D **68**, 046005 (2003).
[20] R. Kallosh and A. D. Linde, J. High Energy Phys. 02 (2007) 002.
[21] J. Fan, M. Reece, and L.-T. Wang, J. High Energy Phys. 09 (2011) 126.
[22] V. Balasubramanian, P. Berglund, J. P. Conlon, and F. Quevedo, J. High Energy Phys. 03 (2005) 007.

[23] M. Cicoli, J. P. Conlon, and F. Quevedo, J. High Energy Phys. 10 (2008) 105.
[24] S. P. Martin, Adv. Ser. Dir. High Energy Phys. **21**, 1 (2010).
[25] L. Randall and R. Sundrum, Nucl. Phys. **B557**, 79 (1999).
[26] G. F. Giudice, M. A. Luty, H. Murayama, and R. Rattazzi, J. High Energy Phys. 12 (1998) 027.
[27] K. Choi, A. Falkowski, H. P. Nilles, M. Olechowski, and S. Pokorski, J. High Energy Phys. 11 (2004) 076.
[28] K. Choi, A. Falkowski, H. P. Nilles, and M. Olechowski, Nucl. Phys. **B718**, 113 (2005).
[29] A. E. Nelson and N. J. Weiner, arXiv:hep-ph/0210288.
[30] R. Sundrum, Phys. Rev. D **71**, 085003 (2005).
[31] K. Hsieh and M. A. Luty, J. High Energy Phys. 06 (2007) 062.
[32] L. L. Everett, I.-W. Kim, P. Ouyang, and K. M. Zurek, J. High Energy Phys. 08 (2008) 102.
[33] M. A. Luty and R. Sundrum, Phys. Rev. D **67**, 045007 (2003).
[34] M. Schmaltz and R. Sundrum, J. High Energy Phys. 11 (2006) 011.
[35] A. Anisimov, M. Dine, M. Graesser, and S. D. Thomas, J. High Energy Phys. 03 (2002) 036.
[36] S. Kachru, J. McGreevy, and P. Svrcek, J. High Energy Phys. 04 (2006) 023.
[37] S. Kachru, L. McAllister, and R. Sundrum, J. High Energy Phys. 10 (2007) 013.
[38] J. D. Wells, Phys. Rev. D **71**, 015013 (2005).
[39] L. J. Hall and Y. Nomura, J. High Energy Phys. 01 (2012) 082.
[40] A. Arvanitaki, N. Craig, S. Dimopoulos, and G. Villadoro, J. High Energy Phys. 02 (2013) 126.
[41] N. Arkani-Hamed, A. Gupta, D. E. Kaplan, N. Weiner, and T. Zorawski, arXiv:1212.6971.
[42] M. Ibe and T. T. Yanagida, Phys. Lett. B **709**, 374 (2012).
[43] M. Ibe, S. Matsumoto, and T. T. Yanagida, Phys. Rev. D **85**, 095011 (2012).
[44] G. B. Gelmini and P. Gondolo, Phys. Rev. D **74**, 023510 (2006).
[45] B. S. Acharya, G. Kane, S. Watson, and P. Kumar, Phys. Rev. D **80**, 083529 (2009).
[46] G. Arcadi and P. Ullio, Phys. Rev. D **84**, 043520 (2011).
[47] T. Moroi, M. Nagai, and M. Takimoto, J. High Energy Phys. 07 (2013) 066.
[48] N. Arkani-Hamed, A. Delgado, and G. F. Giudice, Nucl. Phys. **B741**, 108 (2006).
[49] T. Cohen, M. Lisanti, A. Pierce, and T. R. Slatyer, J. Cosmol. Astropart. Phys. 10 (2013) 061.
[50] J. Fan and M. Reece, J. High Energy Phys. 10 (2013) 124.
[51] M. Endo, K. Hamaguchi, and F. Takahashi, Phys. Rev. Lett. **96**, 211301 (2006).
[52] S. Nakamura and M. Yamaguchi, Phys. Lett. B **638**, 389 (2006).
[53] T. Asaka, S. Nakamura, and M. Yamaguchi, Phys. Rev. D **74**, 023520 (2006).
[54] M. Dine, R. Kitano, A. Morisse, and Y. Shirman, Phys. Rev. D **73**, 123518 (2006).
[55] A. Linde, Y. Mambrini, and K. A. Olive, Phys. Rev. D **85**, 066005 (2012).
[56] J. L. Evans, M. A. G. Garcia, and K. A. Olive, J. Cosmol. Astropart. Phys. 03 (2014) 022.
[57] R. Allahverdi, M. Cicoli, B. Dutta, and K. Sinha, Phys. Rev. D **88**, 095015 (2013).
[58] R. Slansky, Phys. Rep. **79**, 1 (1981).
[59] R. Blumenhagen, M. Cvetic, P. Langacker, and G. Shiu, Annu. Rev. Nucl. Part. Sci. **55**, 71 (2005).
[60] R. Blumenhagen, B. Kors, D. Lust, and S. Stieberger, Phys. Rep. **445**, 1 (2007).
[61] J. L. Feng and J. Kumar, Phys. Rev. Lett. **101**, 231301 (2008).
[62] D. Hooper and K. M. Zurek, Phys. Rev. D **77**, 087302 (2008).
[63] N. Arkani-Hamed and N. Weiner, J. High Energy Phys. 12 (2008) 104.
[64] E. W. Kolb and M. S. Turner, The early universe, Front. Phys. **69**, 1 (1990).
[65] K. Harigaya, M. Kawasaki, K. Mukaida, and M. Yamada, Phys. Rev. D **89**, 083532 (2014).
[66] J. Kaplan, J. High Energy Phys. 10 (2006) 065.
[67] D. J. H. Chung, E. W. Kolb, and A. Riotto, Phys. Rev. D **60**, 063504 (1999).
[68] G. F. Giudice, E. W. Kolb, and A. Riotto, Phys. Rev. D **64**, 023508 (2001).
[69] T. Moroi, arXiv:hep-ph/9503210.
[70] R. Allahverdi, B. Dutta, and K. Sinha, Phys. Rev. D **86**, 095016 (2012).
[71] L. Roszkowski, S. Trojanowski, and K. Turzynski, J. High Energy Phys. 11 (2014) 146.
[72] G. Aad *et al.* (ATLAS Collaboration), Phys. Rev. D **88**, 112006 (2013).
[73] N. de Filippis *et al.* (LEP2 SUSY Working Group; ALEPH, DELPHI, L3, OPAL), http://lepsusy.web.cern.ch/lepsusy/www/inoslowdmsummer02/charginolowdm_pub.html.
[74] T. Gherghetta, G. F. Giudice, and J. D. Wells, Nucl. Phys. **B559**, 27 (1999).
[75] A. Gupta, D. E. Kaplan, and T. Zorawski, J. High Energy Phys. 11 (2013) 149.
[76] P. Gondolo, J. Edsjo, P. Ullio, L. Bergstrom, M. Schelke, and E. A. Baltz, J. Cosmol. Astropart. Phys. 07 (2004) 008.
[77] P. Gondolo, J. Edsjo, P. Ullio, L. Bergstrom, M. Schelke, E. A. Baltz, T. Bringmann, and G. Duda, http://www.darksusy.org.
[78] K. Griest and D. Seckel, Phys. Rev. D **43**, 3191 (1991).
[79] T. Falk, K. A. Olive, and M. Srednicki, Phys. Lett. B **339**, 248 (1994).
[80] M. Srednicki, K. A. Olive, and J. Silk, Nucl. Phys. **B279**, 804 (1987).
[81] D. E. Morrissey, D. Poland, and K. M. Zurek, J. High Energy Phys. 07 (2009) 050.
[82] J. L. Feng, V. Rentala, and Z. Surujon, Phys. Rev. D **84**, 095033 (2011).
[83] J. L. Feng, V. Rentala, and Z. Surujon, Phys. Rev. D **85**, 055003 (2012).
[84] Y. F. Chan, M. Low, D. E. Morrissey, and A. P. Spray, J. High Energy Phys. 05 (2012) 155.
[85] D. E. Morrissey and A. P. Spray, J. High Energy Phys. 06 (2014) 083.
[86] J. D. Bjorken, R. Essig, P. Schuster, and N. Toro, Phys. Rev. D **80**, 075018 (2009).

[87] R. Essig, J. A. Jaros, W. Wester, P. H. Adrian, S. Andreas, T. Averett, O. Baker, and B. Batell *et al.*, arXiv:1311.0029.

[88] J. P. Lees *et al.* (*BABAR* Collaboration), Phys. Rev. Lett. **113**, 201801 (2014).

[89] P. Gondolo and G. Gelmini, Nucl. Phys. **B360**, 145 (1991).

[90] Fermi-LAT Collaboration, http://fermi.gsfc.nasa.gov/ssc/data/access/.

[91] L. Bouchet, E. Jourdain, J. P. Roques, A. Strong, R. Diehl, F. Lebrun, and R. Terrier (INTEGRAL Collaboration), Astrophys. J. **679**, 1315 (2008).

[92] S. C. Kappadath, Ph.D. thesis, University of New Hampshire, 1998.

[93] A. W. Strong, I. V. Moskalenko, and O. Reimer, arXiv:astro-ph/0306346; A. W. Strong, I. V. Moskalenko, and O. Reimer, Astrophys. J. **613**, 962 (2004).

[94] Fermi-LAT Collaboration, Astrophys. J. **750**, 3 (2012).

[95] D. Hooper, C. Kelso, and F. S. Queiroz, Astropart. Phys. **46**, 55 (2013).

[96] R. Essig, E. Kuflik, S. D. Mcdermott, T. Volansky, and K. M. Zurek, J. High Energy Phys. 11 (2013) 193.

[97] N. Padmanabhan and D. P. Finkbeiner, Phys. Rev. D **72**, 023508 (2005).

[98] T. R. Slatyer, N. Padmanabhan, and D. P. Finkbeiner, Phys. Rev. D **80**, 043526 (2009).

[99] P. Meade, M. Papucci, and T. Volansky, J. High Energy Phys. 12 (2009) 052.

[100] D. Hooper, N. Weiner, and W. Xue, Phys. Rev. D **86**, 056009 (2012).

[101] J. F. Navarro, C. S. Frenk, and S. D. M. White, Astrophys. J. **462**, 563 (1996).

[102] J. F. Navarro, E. Hayashi, C. Power, A. R. Jenkins, C. S. Frenk, S. D. M. White, V. Springel, J. Stadel, and T. R. Quinn, Mon. Not. R. Astron. Soc. **349**, 1039 (2004).

[103] V. Springel, J. Wang, M. Vogelsberger, A. Ludlow, A. Jenkins, A. Helmi, J. F. Navarro, C. S. Frenk, and S. D. M. White, Mon. Not. R. Astron. Soc. **391**, 1685 (2008).

[104] G. Hutsi, J. Chluba, A. Hektor, and M. Raidal, Astron. Astrophys. **535**, A26 (2011).

[105] S. Galli, F. Iocco, G. Bertone, and A. Melchiorri, Phys. Rev. D **84**, 027302 (2011).

[106] D. P. Finkbeiner, S. Galli, T. Lin, and T. R. Slatyer, Phys. Rev. D **85**, 043522 (2012).

[107] A. Pomarol and R. Rattazzi, J. High Energy Phys. 05 (1999) 013.

[108] E. Katz, Y. Shadmi, and Y. Shirman, J. High Energy Phys. 08 (1999) 015.

[109] S. Nussinov, Phys. Lett. **165B**, 55 (1985).

[110] S. M. Barr, Phys. Rev. D **44**, 3062 (1991).

[111] D. B. Kaplan, Phys. Rev. Lett. **68**, 741 (1992).

[112] D. E. Kaplan, M. A. Luty, and K. M. Zurek, Phys. Rev. D **79**, 115016 (2009).

[113] M. L. Graesser, I. M. Shoemaker, and L. Vecchi, J. High Energy Phys. 10 (2011) 110.

[114] H. Iminniyaz, M. Drees, and X. Chen, J. Cosmol. Astropart. Phys. 07 (2011) 003.

[115] T. Lin, H. B. Yu, and K. M. Zurek, Phys. Rev. D **85**, 063503 (2012).

[116] N. F. Bell, S. Horiuchi, and I. M. Shoemaker, Phys. Rev. D **91**, 023505 (2015).

[117] H. Davoudiasl, D. E. Morrissey, K. Sigurdson, and S. Tulin, Phys. Rev. Lett. **105**, 211304 (2010).

[118] R. Allahverdi, B. Dutta, and K. Sinha, Phys. Rev. D **83**, 083502 (2011).

[119] N. F. Bell, K. Petraki, I. M. Shoemaker, and R. R. Volkas, Phys. Rev. D **84**, 123505 (2011).

[120] C. Cheung and K. M. Zurek, Phys. Rev. D **84**, 035007 (2011).

[121] G. Kane, J. Shao, S. Watson, and H. B. Yu, J. Cosmol. Astropart. Phys. 11 (2011) 012.

[122] K. M. Zurek, Phys. Rep. **537**, 91 (2014).

[123] W. Fischler, D. Lorshbough, and W. Tangarife, Phys. Rev. D **91**, 025010 (2015).

[124] N. Blinov, D. E. Morrissey, K. Sigurdson, and S. Tulin, Phys. Rev. D **86**, 095021 (2012).

[125] D. S. Akerib *et al.* (LUX Collaboration), Phys. Rev. Lett. **112**, 091303 (2014).

[126] J. Angle *et al.* (XENON10 Collaboration), Phys. Rev. Lett. **107**, 051301 (2011); **110**, 249901(E) (2013).

[127] R. Agnese *et al.* (SuperCDMSSoudan Collaboration), Phys. Rev. Lett. **112**, 041302 (2014).

[128] G. Angloher, S. Cooper, R. Keeling, H. Kraus, J. Marchese, Y. A. Ramachers, M. Bruckmayer, and C. Cozzini *et al.*, Astropart. Phys. **18**, 43 (2002).

[129] J. L. Feng and Y. Shadmi, Phys. Rev. D **83**, 095011 (2011).

[130] K. K. Boddy, J. L. Feng, M. Kaplinghat, and T. M. P. Tait, Phys. Rev. D **89**, 115017 (2014).

[131] T. Appelquist and H. D. Politzer, Phys. Rev. Lett. **34**, 43 (1975).

[132] S. J. Brodsky, J. F. Gunion, and D. E. Soper, Phys. Rev. D **36**, 2710 (1987).

[133] H. Baer, K.-m. Cheung, and J. F. Gunion, Phys. Rev. D **59**, 075002 (1999).

[134] R. H. Cyburt, B. D. Fields, K. A. Olive, and E. Skillman, Astropart. Phys. **23**, 313 (2005).

[135] G. Mangano and P. D. Serpico, Phys. Lett. B **701**, 296 (2011).

[136] E. Di Valentino, A. Melchiorri, and O. Mena, J. Cosmol. Astropart. Phys. 11 (2013) 018.

[137] L. Ackerman, M. R. Buckley, S. M. Carroll, and M. Kamionkowski, Phys. Rev. D **79**, 023519 (2009).

[138] J. L. Feng, M. Kaplinghat, H. Tu, and H.-B. Yu, J. Cosmol. Astropart. Phys. 07 (2009) 004.

[139] M. R. Buckley and P. J. Fox, Phys. Rev. D **81**, 083522 (2010).

[140] M. Rocha, A. H. G. Peter, J. S. Bullock, M. Kaplinghat, S. Garrison-Kimmel, J. Onorbe, and L. A. Moustakas, Mon. Not. R. Astron. Soc. **430**, 81 (2013).

[141] A. H. G. Peter, M. Rocha, J. S. Bullock, and M. Kaplinghat, Mon. Not. R. Astron. Soc. **430**, 105 (2013).

[142] M. Vogelsberger, J. Zavala, and A. Loeb, Mon. Not. R. Astron. Soc. **423**, 3740 (2012).

[143] J. Zavala, M. Vogelsberger, and M. G. Walker, Mon. Not. R Astron. Soc. Lett. **431**, L20 (2013).

[144] D. J. Gross, R. D. Pisarski, and L. G. Yaffe, Rev. Mod. Phys. **53**, 43 (1981).

[145] L. D. McLerran, Rev. Mod. Phys. **58**, 1021 (1986).

[146] P. B. Arnold and L. G. Yaffe, Phys. Rev. D **52**, 7208 (1995).

[147] S. Tulin, H.-B. Yu, and K. M. Zurek, Phys. Rev. D **87**, 115007 (2013).
[148] D. V. Nanopoulos, S. Ono, and T. Yanagida, Phys. Lett. **137B**, 363 (1984).
[149] J. H. Kuhn and S. Ono, Phys. Lett. **142B**, 436 (1984).
[150] J. T. Goldman and H. Haber, Physica (Amsterdam) **15D**, 181 (1985).
[151] F.-Y. Cyr-Racine, R. de Putter, A. Raccanelli, and K. Sigurdson, Phys. Rev. D **89**, 063517 (2014).
[152] S. L. Dubovsky, D. S. Gorbunov, and G. I. Rubtsov, Pis'ma Zh. Eksp. Teor. Fiz. **79**, 3 (2004) [JETP Lett. **79**, 1 (2004)].
[153] A. D. Dolgov, S. L. Dubovsky, G. I. Rubtsov, and I. I. Tkachev, Phys. Rev. D **88**, 117701 (2013).
[154] J. Fan, A. Katz, L. Randall, and M. Reece, Phys. Dark Univ. **2**, 139 (2013).
[155] M. Kawasaki, K. Kohri, and T. Moroi, Phys. Rev. D **71**, 083502 (2005).
[156] K. Jedamzik, Phys. Rev. D **74**, 103509 (2006).